



NOVA

University of Newcastle Research Online

nova.newcastle.edu.au

Dickinson, J.E. & Galvin, K.P. 'Fluidized bed desliming in fine particle flotation – Part I', *Chemical Engineering Science*, 108, 283-298 (2014)

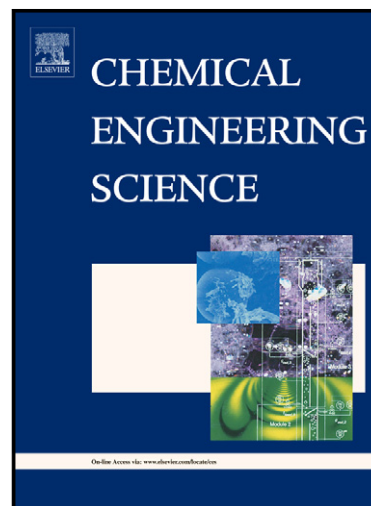
Available from: <http://dx.doi.org/10.1016/j.ces.2013.11.006>

Accessed from: <http://hdl.handle.net/1959.13/1042794>

Author's Accepted Manuscript

Fluidized Bed Desliming in Fine Particle Flotation – Part I

J.E. Dickinson, K.P. Galvin



www.elsevier.com/locate/ces

PII: S0009-2509(13)00735-5
DOI: <http://dx.doi.org/10.1016/j.ces.2013.11.006>
Reference: CES11386

To appear in: *Chemical Engineering Science*

Received date: 5 August 2013
Revised date: 23 October 2013
Accepted date: 2 November 2013

Cite this article as: J.E. Dickinson, K.P. Galvin, Fluidized Bed Desliming in Fine Particle Flotation – Part I, *Chemical Engineering Science*, <http://dx.doi.org/10.1016/j.ces.2013.11.006>

This is a PDF file of an unedited manuscript that has been accepted for publication. As a service to our customers we are providing this early version of the manuscript. The manuscript will undergo copyediting, typesetting, and review of the resulting galley proof before it is published in its final citable form. Please note that during the production process errors may be discovered which could affect the content, and all legal disclaimers that apply to the journal pertain.

Fluidized Bed Desliming in Fine Particle Flotation – Part I**J.E. Dickinson* and K.P. Galvin****Centre for Advanced Particle Processing and Transport, Newcastle Institute for Energy
and Resources, The University of Newcastle, Callaghan, NSW 2308, Australia****Abstract**

This is the first of a series of publications concerned with a novel system that transforms the hydrodynamics of flotation. This system, referred to as a Reflux Flotation Cell, consists of a vertical flotation zone, with a system of parallel inclined channels below. The system is enclosed at the top by a fluidization distributor, while a central port is used to discharge the overflow product. The inclined channels located below the vertical section enhance the segregation of the bubbles from the tailings flow, permitting separations to be conducted at bubble surface fluxes well beyond the normal flooding condition, while also permitting extreme wash water fluxes. The system hydrodynamics produces spherical bubbly-foam, with a bubble volume fraction of order 0.5, ideal for counter-current washing, and hence desliming.

This paper addresses two objectives. The first concerns the fluidization boundary condition at the top of the device. We identify for the first time a conundrum that arises when Drift Flux theory and fluidization theory are used to describe the effect of wash water addition in flotation. A subtle but nevertheless significant change in the predicted bias flux arises when the system is formally fluidized, resulting in the wash water reporting with the overflow, and

* Corresponding author: Tel: +61 2 4033 9088; Fax: +61 2 4033 9095.
E-mail address: Jamie.Dickinson@newcastle.edu.au

hence failing to provide the desired desliming. Our experimental work, however, demonstrated that the applied fluidization leads to strong positive bias, with a downwards liquid flux and in turn powerful desliming of hydrophilic particles. Indeed the system behaved as though the wash water was introduced below rather than at the upper boundary.

The second, and most important objective was to assess the system hydrodynamics with respect to extreme gas and wash water fluxes using firstly a particle-free system, and secondly assess the desliming achievable using a system containing hydrophilic particles. Thus in Part I the system was free of hydrophobic particles. The enhanced bubble-liquid segregation arising from the system of inclined channels permitted very high gas fluxes, sufficient to achieve a bubble surface flux of $144 \text{ m}^2/\text{m}^2\text{s}$, well beyond the theoretical flooding limit of $\sim 100 \text{ m}^2/\text{m}^2\text{s}$ (Wace et al., 1968). This high bubble surface flux was especially significant given this occurred during the application of extreme bias fluxes, as high as 2.5 cm/s passing downwards. Experiments involving a silica feed were used to quantify the performance of the desliming, covering extreme gas and fluidization (wash) water fluxes. Silica rejection from the product exceeded 99 %.

Keywords: Flotation, Desliming, Drift Flux, Inclined Channels, Fluidization, Bubble Column.

1. Introduction

Flotation is used extensively in the recovery of valuable minerals and coal. The conventional flotation process involves the transport of particle-laden bubbles up through a dispersed and dilute bubbly zone to form a foam zone, rich in hydrophobic particles. A distinct interface

separates these two zones. Entrainment of ultrafine hydrophilic particles, known as slimes, into the foam has a severe and negative impact on the product grade. A foam zone provides an effective method for promoting water rejection and, in turn, slimes rejection. To improve the product grade, wash water is often sprayed onto the free-surface (top layer) of the foam to wash the entrained slimes down through the foam. Alternatively, the wash water can be injected into the foam beneath the free-surface. Either way it is very difficult to achieve uniform drainage of the wash water down through the foam given the tendency for water to also report directly with the product, or for the water to rupture the foam and achieve very little. Much of this difficulty arises due to the poor permeability of a foam.

Of specific interest in this study is the direction of the interstitial water flow through the system of rising bubbles and foam, and its influence on the slimes yield reporting to the product overflow. To ensure the effectiveness of wash water in removing slimes, a net downward flow of liquid through the foam and bubbly zones, or a positive bias, is essential (Finch and Dobby, 1990). In conventional flotation cells, such as mechanical cells and flotation columns, or even Jameson cells, the capacity to deslime using wash water is limited by the hydrodynamics of maintaining a stable foam, identified by distinct bubbly (collection) and foam (cleaning) zones.

The objective of this study was to address the present hydrodynamic limitations of conventional flotation. Drift Flux theory (Wallis, 1969), examined in the next section, provides a theoretical framework for interpreting the effects of increasing gas and wash water fluxes on the wash water bias, and hence the desliming. When the gas flux is progressively increased the effectiveness of wash water delivered from above the free-surface is reduced. A further increase in the gas flux leads to a state of flooding, resulting in the loss of the

interface between the lower bubbly zone and the upper foam zone. Separation becomes impossible as the tailings stream begins to resemble the product stream.

These limitations are addressed here using a Reflux Classifier (Galvin et al., 2012; 2010), inverted in order to form the Reflux Flotation Cell (RFC). Figure 1 provides a schematic representation. The upper section of the RFC consists of an enclosed fluidization distributor, thus replacing the free-surface that exists above conventional flotation devices. The incorporation of the enclosed top confines the foam, or bubbly-liquid product, to discharge through an outlet of reduced area relative to the cross section of the cell. The inclusion of a system of parallel inclined channels, which increases the segregation rate (Boycott, 1920; Nakamura and Kuroda, 1937; Ponder, 1925) of the bubbles from the tailings flow, is used to prevent the loss of bubbles, and attached particles, from reporting to the tailings stream. Thus the RFC is designed to tolerate much higher gas and wash water fluxes. In turn this system challenges the existing paradigm of flotation - the need to always operate with foam to reject water, and in turn reject the slimes from the product. Rather, a highly permeable bubbly zone can be established at high gas fluxes, with a volume fraction of bubbles of order 0.5, ideal for desliming.

The focus of this study was on (i) the hydrodynamics of the RFC and (ii) the associated desliming of hydrophilic particles from the product stream. The hydrodynamics are explored theoretically in Section 2 using Drift Flux and fluidization theory, and experimentally by examining the implications of the novel fluidization boundary condition. The desliming is then investigated experimentally using a model feed consisting of fine hydrophilic silica particles to evaluate the extent of the desliming using fluidization water. Specifically the focus was on the rejection of the silica as slimes rather than on the true flotation of valuable

particles. Hence, no hydrophobic particles were included in this study. The separate question of hydrophobic particle recovery in conjunction with hydrophilic particle rejection will be examined in a forthcoming paper, referred to as Part II (Galvin and Dickinson, 2013).

2. Theoretical

Consider the continuous operation of a flotation cell configured as an inverted gravity separation system in which the top of the cell is enclosed to confine the overflow to a narrow discharge port. Figure 2 shows the general arrangement. Discharge of the gas flux, j_g , and associated liquid flux (j_f or \hat{j}_f) proceeds through the upper port as foam and assumed to occur iso-kinetically. The volumetric flow rate of foam emerging from the vessel, per unit of vessel area, is referred to as the overflow velocity, V_{OF} .

The entering gas rises as a dispersed system of bubbles at a relatively low volume fraction, referred to as a dilute bubbly zone. Above this zone the gas rises up through the remainder of the system as foam, discharging through the upper system port. The sharp interface, which exists between these two zones, can be maintained at a fixed elevation through adjustment of the tailings discharge rate. As the gas flux increases the volume fraction of the gas in the bubbly zone increases, while the volume fraction of the gas in the foam zone decreases. Flooding occurs when the volume fraction of the gas above and below the interface becomes the same, and hence the interface disappears. In conventional flotation the flooding condition must be avoided by limiting the gas flux to levels well below this flooding limit. When wash water is introduced into the foam below the free-surface, a so-called “wet” foam of lower gas volume fraction forms below the injection point, while the foam above the injection point recovers and hence, in principle, remains unaffected by the wash water injection. In turn, when wash water is introduced and a “wet” foam formed, flooding is reached at a lower gas

flux. It should be noted that in the extreme the “wet” foam state approaches that of a spherical foam, described here as a concentrated bubbly zone. In the Reflux Flotation Cell the system can be operated beyond the flooding condition due to the enhanced segregation achieved between the bubbles and the tailings flow within the inclined channels, with the volume fraction of the gas within the bubbly zone at relatively high levels of order 0.5. This action, however, is not considered as part of the Drift Flux analysis in this section. Hence the analysis is limited to gas fluxes below the flooding limit.

Figure 2 shows four steady state systems of rising foam driven by a gas flux, j_g . Any input into the system is given by an arrow pointing into the system, with a positive value assigned for that direction. Similarly, any output from the system is given by an arrow pointing out of the system, with a positive value assigned for that direction. Fluidization wash water is supplied at a flux, j_w , in Figures 2b, 2c, and 2d. The wash water flux, j_w , is an input with an assigned positive value. Once this flux, j_w , enters the system, we apply the convention used by others (Dobby and Finch, 1990) to describe the liquid flux above and below this injection point. The superficial liquid velocity, j_f , above the wash water injection point is taken to be positive in the upwards direction. While, the superficial liquid velocity, j_b , below the wash water injection point, referred to as the bias flux, j_b , is taken to be positive in the downwards direction. It is noted however, that at all elevations the interstitial liquid velocity, u_L , and the bubble rise velocity, u_b , are taken to be positive in the upwards direction. The superficial gas velocity, j_g , is also taken to be positive in the upwards direction.

Figure 2a involves no fluidization, Figure 2b involves wash water addition at a set distance below the upper system boundary, Figure 2c involves fluidization at the upper system boundary at low gas fluxes, and Figure 2d involves fluidization at the upper system boundary

at high gas fluxes. In Figure 2c the system is said to be unconstrained by the flux curve, while in Figure 2d the system is flux curve constrained. This concept of a flux curve constrained or unconstrained system is discussed in the following sections.

The well-known model of Richardson and Zaki (1954), used to describe batch settling or fluidization, can be used to describe the effects of “hindered settling” on a rising bubble. That is,

$$V_s = V_t(1-\theta)^n \quad (1)$$

where V_s denotes the bubble velocity relative to the vessel in the absence of fluidization, and θ is the volume fraction of the dispersed gas phase. V_t is the terminal rise velocity of a single bubble in an infinite medium, hence liquid drainage through the foam is considered to be gravity-dominated. Note that, in general, capillary suction only plays a dominant role within thin boundary layers, such as along a sloping weir (Grassia et al., 2002), and is therefore considered to be insignificant in this one-dimensional analysis. The corresponding relationship for the slip velocity, V_{slip} , of a spherical bubble, is

$$V_{slip} = V_t(1-\theta)^{n-1}. \quad (2)$$

Other characteristic equations can be used to account for surface mobility and bubble deformity if necessary (Stevenson et al., 2007; Zhou and Egiebor, 1993). The exponent n is highly dependent on the nature of the discrete phase.

2.1 Flux Curve Constrained Flotation

This section outlines the application of Drift Flux theory to flotation and what is meant by flux curve constrained flotation. For some readers it will be useful to firstly consider the

analogous arrangement of a continuous steady state thickener, which is outlined in Appendix A. An equivalent approach is applied here in terms of the present problem concerned with the production of foam. A basic treatment is provided hence there is no wash water or fluidization applied to the foam. We begin by describing the system under batch conditions, then under continuous steady state conditions, and then discuss these conditions using an operating line on a flux curve.

In the first instance the vessel is closed at the top, as shown in Part (i) of Figure 3A, and it is assumed that liquid is added or removed from below so as to preserve the total system volume. In this case the gas flux, j_g , is imposed from below, forming a low concentration of rising gas bubbles which deposit at the top to form foam. The bubbles are resilient, and hence never coalesce, and are assumed to be incompressible, and spherical.

The theory of Kynch (1952) predicts the formation of concentration waves that travel downwards through the foam at a propagation velocity given by,

$$V_p = -\frac{d(V_s \theta)}{d\theta}. \quad (3)$$

Note that here V_p is numerically positive in the downwards direction while the settling velocity of the bubbles, V_s , is numerically positive in the upwards direction. The downwards velocity of the foam, however, is given by the maximum propagation velocity that can be sustained by the feed flux, j_g . We thus assign the specific term, V_{pb} , to denote this maximum downwards velocity of the foam, the key focus of our analysis. We also assign the specific term, V_{sb} , to denote the rise velocity of the bubbles that are present just inside the surface of the foam.

If the gas flux was suddenly switched off the observer would witness the overall height of the foam decrease at the velocity, V_{sb} , due to the on-going foam drainage or bubble rise. Thus the imposed gas flux, j_g , is responsible for “making up” for the reduction in height plus the increase in height per unit time, $V_{sb}+|V_{pb}|$. The volume fraction of bubbles just inside the surface of the foam is θ_b . Thus the imposed gas flux, j_g , is related to the rise velocity of the bubbles just inside the foam and the corresponding propagation velocity, according to,

$$j_g = (|V_{pb}| + V_{sb})\theta_b. \quad (4)$$

Higher concentrations are present within the foam, increasing in value towards the top of the system, and clearly propagate at velocities lower in magnitude than the value of $|V_{pb}|$ at θ_b . When the top of the system is finally opened, as shown in Part (ii) of Figure 3A, and the interface between the rising bubbles and foam becomes fixed, the foam escapes at an overflow velocity, $V_{OF} = |V_{pb}|$. Given that the rise velocities of all other concentrations within the foam must have been lower in magnitude than the magnitude of the original downwards velocity of the foam, $|V_{pb}|$, and given that the overflow velocity imposes an upwards velocity given by the magnitude $|V_{pb}|$, these higher concentrations now propagate upwards and out of the system, leaving just one constant concentration within the foam, θ_b .

By permitting an overflow velocity equal in magnitude to $|V_{pb}|$, it is possible to achieve continuous steady state production of foam, with a fixed interface position between the dilute bubbly zone and the foam zone. A small disturbance can easily lead to a rise or a fall in the interface level, so some effort is needed to keep the interface fixed. At this point the volume flux of gas, j_g , and the volume flux of liquid, j_f , transported up through both the zone of rising bubbles and foam are fixed and equal in magnitude to the flux of gas and liquid emerging via the overflow. This volumetric overflow flux matches the magnitude of the original propagation velocity of the foam, $|V_{pb}|$. Therefore,

$$|V_{pb}| = j_g + j_f. \quad (5)$$

The above discussion is readily quantified using an appropriate flux curve construction. The settling flux of the bubbles is given by the product of the settling velocity, V_s , and volume fraction of bubbles, θ . The basis of this velocity, V_s , as applied to the bubbles, is defined by Equation 1. We have chosen to normalize the flux curve with respect to the particle terminal velocity, V_t . We have also assumed a value for $n = 2$ in Equation 1, despite the fact that for the relatively “wet” foams used in this study the value will normally be larger. In fact the value obtained in this study was $n = 3.2$. The lower value of $n = 2$ has been used because it provides a much clearer illustration of the detailed flux curve construction.

Figure 3B shows the flux curve produced using a plot of the settling flux of the bubbles, $V_s\theta$, versus the volume fraction of bubbles, θ . The flux curve is normalized using the bubble terminal velocity, V_t . However, in the following discussion the normalization is neglected in order to simplify the description. A Yoshioka flux curve construction (Fitch, 1979), consisting of an operating line extending from the imposed gas feed flux, j_g , on the vertical axis down to the flux curve, as a tangent, is shown. The tangent occurs at the volume fraction, θ_b , which is the volume fraction of the bubbles just inside the surface of the foam. Further, the slope of the tangent is the corresponding propagation velocity, V_{pb} , which is the downwards velocity of the foam in the absence of any overflow removal. This is the maximum propagation velocity that can be sustained by the gas feed flux, j_g , and hence this tangent condition governs the properties of the foam surface. In order to achieve steady state, an overflow velocity, V_{OF} , is imposed equal in magnitude and opposite in direction to the propagation velocity, V_{pb} , of the foam. The tangent intersects the horizontal axis at the steady

state overflow concentration, θ_{OF} . This volume fraction is higher in value than the internal system volume fraction, θ_b .

In the absence of fluidization (i.e. with no wash water) there is always a step change from the internal system concentration to that of the final exit concentration, θ_{OF} (Fitch, 1979). Just prior to the final boundary there is a finite settling velocity relative to the vessel, V_{sb} , however at the final boundary there is suddenly no further settling that is possible. This overall step change in velocity (from $V_{sb} + V_{OF}$ to V_{OF}) generates the step change in concentration (from θ_b to θ_{OF}), in accordance with the requirements for a steady state material balance, $(V_{sb} + V_{OF})\theta_b = V_{OF}\theta_{OF}$.

The slope of the chord from the origin to the point at which the tangent meets the flux curve is clearly V_{sb} . Thus, in accordance with Equation 4, the imposed gas flux, j_g , establishes a propagation flux component, $|V_{pb}|\theta_b$ and settling flux component, $V_{sb}\theta_b$. At steady state it is necessary for both of these components to be transported through the system to the overflow.

In the Appendix a modified flux curve construction is also presented, showing that the tangent condition represents a “bottle-neck” in the transport of particles (in this case gas bubbles) through the system. This “bottle-neck” denotes the maximum gas flux that can be transported to the overflow at this overflow velocity. At lower gas fluxes the system is unconstrained by the flux curve, given the transport of this gas flux is independent of the flux curve. However, the transport is flux curve constrained at higher gas fluxes.

The propagation velocity, V_p , can be calculated using Equation 3 by obtaining the slope of the relevant flux curve, and then incorporating Equation 1. Application of the product rule gives,

$$V_p = -V_s - \frac{\theta V_t d(1-\theta)^n}{d\theta}. \quad (6)$$

It follows that,

$$V_p = -V_s + \theta V_t n(1-\theta)^{n-1}. \quad (7)$$

Incorporating Equation 1 again and inserting the specific velocities and the concentration which applies to the foam at the interface, gives

$$V_{pb} = -V_{sb} + \frac{\theta_b n V_{sb}}{(1-\theta_b)}. \quad (8)$$

Combining this result with Equation 4 provides an established relationship between the imposed gas flux, j_g , and the equilibrium volume fraction of the bubbles. That is,

$$\frac{V_{sb}}{j_g} = \frac{(1-\theta_b)}{n\theta_b^2}. \quad (9)$$

It is noted that in any Equation involving the exponent, n , the result is limited to the specific hindered settling description given by Equation 1. All other Equations have no such restriction.

An explicit solution is obtained by specifying the value of θ_b , inserting this value into Equation 1 to obtain V_{sb} , and then substituting these quantities and the exponent n into Equation 9 to obtain j_g . Our preference however, is to use an implicit iterative approach to obtain θ_b for a given gas flux, j_g .

Eliminating V_{pb} from Equations 4 and 5, and combining the result with Equation 9, gives

$$\frac{j_f}{j_g} = \frac{(1-\theta_b)}{\theta_b} - \frac{(1-\theta_b)}{\theta_b^2 n}. \quad (10)$$

Thus Equations 9 and 10 provide a direct measure of the liquid flux, j_f , that rises up through a flux curve constrained system.

This system can be made to operate in a manner that is unconstrained by the flux curve. This occurs when the interface between the dilute bubbly zone and foam zone is allowed to rise upwards, through an increase in the overflow velocity, V_{OF} (for a given gas flux). The foam zone is then lost from the system, leaving behind the dilute bubbly zone. This condition involves a specific overflow velocity of gas and liquid. At this overflow velocity, and at this gas flux, the system is unconstrained by the flux curve. This is because at this overflow velocity additional gas flux can still be transported to the overflow, regardless of the flux curve. But when the gas flux increases sufficiently (for a given overflow flux), the interface between the dilute bubbly zone and foam suddenly reappears, with the foam zone propagating downwards. The system is then flux curve constrained, as the gas flux transported to the overflow is constrained by the flux curve. The overflow velocity must be further increased in order to accommodate this higher gas flux at steady state.

2.2 Wash Water Injected into the Foam

Figure 2b depicts the inverted fluidized bed system operated with no fluidization water through the distributor. Rather, wash water is injected at an elevation well below the upper boundary. If we define a control volume around the upper portion there is plainly no difference between the upper parts of Figure 2a and Figure 2b. Moreover, both systems are flux curve constrained.

The systems are operated at the same gas flux, and must have the same bubble volume fraction in the upper section. Thus, the liquid flux, j_f , rising up through the cell, from above the elevation of the wash water injection, must also be the same. This means that none of the added wash water rises with the foam. By convention, we define the bias flux, j_b , as a positive vector in the downwards direction as shown in Figure 2b. Hence, the bias flux just below the injection point is given by,

$$j_b = j_w - j_f \quad (11)$$

while a fixed upwards flux, j_f , forms from above the injection point. Thus there is a distinct step change in the bubble volume fraction across the injection point.

In order to understand the state of the system below the point of wash water injection, we first need to describe the conditions above this zone. Thus we can use Equations 9 and 10, which apply to the zone above the wash water injection in Figure 2b, to obtain the liquid flux above the injection point, j_f , and in turn the bias flux, j_b , that develops below the wash water injection point in Figure 2b.

The interstitial liquid of volume fraction, θ_L , in the zone below the wash water injection has a velocity, u_L , which is positive in the upwards direction. Thus,

$$j_b = -u_L \theta_L. \quad (12)$$

Combining Equations 11 and 12 gives,

$$j_w - j_f = -u_L \theta_L. \quad (13)$$

The volume fraction of the bubbles in the “wet” foam below the wash water injection in Figure 2b, θ_w , needs to be determined by applying a flux balance in this lower zone. The total flux in the upwards direction is,

$$\psi_T = j_g - j_b = j_g + j_f - j_w. \quad (14)$$

The total flux is also given by the sum of the bubble flux and the liquid flux. That is,

$$\psi_T = u_b \theta_w + u_L \theta_L. \quad (15)$$

Here, u_b is the rise velocity of the bubbles relative to the vessel in the zone below the water injection, u_L is the interstitial liquid velocity in the zone below the water injection, defined as positive in the upwards direction, and $\theta_L = (1 - \theta_w)$ is the corresponding volume fraction of the liquid. Eliminating the total flux from Equations 14 and 15 gives,

$$j_g + j_f - j_w = u_b \theta_w + u_L (1 - \theta_w). \quad (16)$$

Equation 16 becomes,

$$j_g + j_f - j_w = (u_b - u_L) \theta_w + u_L. \quad (17)$$

The slip velocity, given by,

$$V_{slip} = u_b - u_L \quad (18)$$

is evaluated at the bubble volume fraction, θ_w . Substitution into Equation 17 gives,

$$j_g + j_f - j_w = V_{slip} \theta_w + u_L. \quad (19)$$

Rearranging Equation 13 provides an expression for the interstitial liquid velocity. That is,

$$u_L = (j_f - j_w) / (1 - \theta_w). \quad (20)$$

Thus the interstitial liquid velocity can be eliminated from Equations 19 and 20, giving

$$(j_g + j_f - j_w)(1 - \theta_w) = V_{slip} \theta_w (1 - \theta_w) + (j_f - j_w). \quad (21)$$

It then follows that,

$$j_g (1 - \theta_w) = V_{slip} \theta_w (1 - \theta_w) + (j_f - j_w) \theta_w. \quad (22)$$

Incorporating Equations 1 and 2,

$$j_g (1 - \theta_w) = V_s \theta_w + (j_f - j_w) \theta_w. \quad (23)$$

It is noted that V_s must be evaluated at the lower bubble volume fraction, θ_w . In summary, Equations 9 and 10 are used to obtain the value of θ_b and j_f in the zone above the water

injection. In turn Equations 11 and 23 are used respectively to obtain the bias flux and bubble volume fraction, θ_w , below the water injection.

2.3 Fluidization through the Upper Boundary

In this section we examine for the first time a subtle but important issue associated with the boundary condition at the upper surface of the flotation vessel. The system, shown in Figure 2c, is subjected to inverted fluidization at a fixed and significant flux of liquid down through the upper boundary. Figure 4 shows different scenarios that are discussed below.

In the first instance the upper boundary is closed, and hence there is no discharge of foam. The rest of the system remains full, by either discharging or adding liquid as required. Imagine if the system was supplied with an exceedingly low flux of gas bubbles from below. These would rise up through the vertical section, accumulating at the top over a long period of time. A fluidized bed of bubbles would then be formed in the upper section, with the bed height increasing in the downwards direction very slowly with time. The bed concentration of bubbles, governed entirely by the fluidization flux, would be uniform in nature from the upper boundary condition down through the bed.

Consider now the discharge of bubbly liquid through the upper boundary of the system. Here the fluidization is assumed to be sufficient to generate a relatively “wet” foam state known as spherical foam, essentially a concentrated bubbly zone. By permitting a sufficient rate of discharge, a constant fluidized bed height would eventually be established. Then the gas flux entering would equal the gas flux leaving. At this point in time a downwards positive bias

must exist, almost equal to the fluidization flux, given the liquid discharge via the concentrated bubbly flow would be exceedingly low in comparison to the significant fluidization velocity.

Of course, by increasing the gas flux to a significant level it is necessary to discharge the concentrated bubbly flow at a much higher rate in order to preserve the bed height. Each additional bubble discharges with a finite quantity of liquid. At this point the bed concentration of bubbles would continue to be uniform from the upper boundary condition down through the vessel, governed entirely by the fluidization flux. A downwards positive bias would still exist, but would be much smaller in magnitude than before due to the now significant discharge flux of concentrated bubbly liquid.

Eventually, with a sufficiently high gas flux, the liquid discharge flux associated with the concentrated bubbly flow out of the top of the vessel would match the fluidization flux, and hence the bias would become zero. At some higher gas flux, however, the system will become flux curve constrained. Under this condition, the concentrated bubbly liquid discharge flux required to maintain a steady bed height would be so high that the downwards bias flux would in fact become negative. This liquid flux within the system is of course a positive liquid flux, j_f , in the upwards direction, predicted directly using Drift Flux theory. Under these conditions the fluidization flux supplied to the system fails to provide positive bias, reporting instead to the overflow with the concentrated bubbly discharge flow. Thus when the system becomes flux curve constrained, the fluidization flux simply reports to the overflow resulting in a more dilute overflow than would have existed in the absence of fluidization.

A modified flux curve is produced by incorporating the specific level of wash water fluidization, j_w . This fluidization produces a change in the bubble settling velocity relative to the vessel. Thus the relevant bubble velocity for producing this flux curve is $V_s - j_w$ and hence the relevant flux curve involves a plot of $\theta(V_s - j_w)$ versus θ . Figure 5 shows the flux curve normalized by the terminal velocity, V_t , with $n = 2$ and $j_w/V_t = 0.025$. Note, values used in the construction of the flux curve were selected for illustrative purposes only and should not be interpreted with reference to the experimental work.

The state of fluidization results in the upward bubble velocity, in the absence of fluidization, V_s , matching the downwards fluidization velocity, j_w . Incorporating Equation 1 into this balance then establishes the value of the bubble volume fraction, θ_0 . That is,

$$V_s = j_w = V_t(1 - \theta_0)^n. \quad (24)$$

Under these conditions the concentration, θ_0 , will exist throughout the bed, and will also equal the value of the overflow concentration, θ_{OF} . That is,

$$\theta_0 = \theta_{OF} = 1 - \sqrt[n]{\frac{j_w}{V_t}}. \quad (25)$$

For this fluidized bed case the settling velocity is balanced by the fluidization velocity and hence there is no step change in either velocity or concentration at the system boundary. Thus, $\theta_0 = \theta_{OF}$. At a higher gas flux the system becomes flux curve constrained, and a step change emerges.

The feed operating line, based on $j_g^*/V_t = 0.224$, forms a tangent to the flux curve and intersects the flux curve along the x-axis at θ_0 . This tangent condition provides the upper limit for flotation unconstrained by the flux curve. Substituting Equation 25 into Equation 9 provides the minimum gas flux, j_g^* , necessary for flux curve constrained operation.

As noted above, the system is unconstrained by the flux curve when the value of the gas flux, j_g is below the value of j_g^* . Figure 5 shows a series of operating lines that intersect at gas flux values below this level. Here the operating lines depend on only the fluidization flux and the gas flux, and hence are independent of the flux curve. The total overflow flux of liquid and gas, $\hat{j}_f + j_g$, must equate with the quantity, $\frac{j_g}{\theta_{OF}}$, where θ_{OF} is the overflow volume fraction of bubbles. Hence,

$$\hat{j}_f + j_g = \frac{j_g}{\theta_{OF}}. \quad (26)$$

For a system unconstrained by the flux curve, the net downwards flux of liquid, or liquid bias flux, j_b , is therefore,

$$j_b = j_w - \hat{j}_f = j_w - j_g \left(\frac{1 - \theta_{OF}}{\theta_{OF}} \right). \quad (27)$$

Finally, we consider what happens when the fluidized system becomes flux curve constrained, with the imposed gas flux, j_g , greater than the gas flux, j_g^* . Figure 2d illustrates this case. The flux curve, modified by the fluidization flux, j_w , involves a plot of $(V_s - j_w)\theta$ versus θ . Figure 6 shows the flux curve normalized using the terminal velocity, V_t , and modified by the normalized fluidization flux, $j_w/V_t = 0.025$. This function can be differentiated to obtain the modified propagation velocity. That is,

$$\hat{V}_p = -\frac{d[(V_s - j_w)\theta]}{d\theta}. \quad (28)$$

Applying the product rule gives,

$$\hat{V}_p = -[V_s - j_w] - \frac{dV_s}{d\theta}. \quad (29)$$

Equation 29 is equivalent to,

$$\hat{V}_p = j_w - \frac{d(V_s\theta)}{d\theta}. \quad (30)$$

Thus the modified propagation velocity is equal to the standard propagation velocity, V_p , given by Equation 3 plus the fluidization flux, j_w . Thus,

$$\hat{V}_p = -\frac{d[(V_s - j_w)\theta]}{d\theta} = V_p + j_w. \quad (31)$$

Equation 31 shows that to maintain a fixed interface between the dilute bubbly zone and “wet” foam zone it is necessary to establish an overflow flux of magnitude equal to the propagation velocity, $|\hat{V}_{pb}| = |V_{pb}| + |j_w|$. This means the overflow flux is larger in magnitude than the usual value, $|V_{pb}|$, by an amount, $|j_w|$. Hence the added fluidization flux reports directly to the overflow, and is not directed downwards. This finding is also consistent with an assessment of the propagation and settling flux components. The gas flux, j_g , fed to the system can again be split into its propagation and “settling” flux components, giving

$$j_g = |\hat{V}_{pb}| \hat{\theta}_b + (V_{sb} - j_w) \hat{\theta}_b = (|V_{pb}| + V_{sb}) \hat{\theta}_b. \quad (32)$$

We have used the term $\hat{\theta}_b$ to denote the relevant volume fraction of bubbles in the upper zone. The right hand side of Equation 32 is equivalent to the result that applies in the absence of fluidization, given by Equation 4. Thus an important observation here is that for flux curve constrained systems the steady state volume fraction of bubbles in the upper zone, θ_b , in Figure 2a is the same as the steady state volume fraction of bubbles, $\hat{\theta}_b$, in Figure 2d. In other words, the bubble volume fraction in the upper section, $\theta_b = \hat{\theta}_b$, is independent of the fluidization flux, j_w , and identical to the result obtained in the absence of any fluidization.

Clearly the volume fraction of the bubbles in the foam is not influenced by the fluidization flux when the system is flux curve constrained. It also follows that the liquid flux, j_f , transported up through the foam is not influenced by the fluidization flux. Thus the imposed fluidization flux, j_w , joins the rising flux of liquid, j_f , producing the total overflow flux, \hat{j}_f . Therefore,

$$\hat{j}_f = j_f + j_w. \quad (33)$$

Equation 33 shows that the fluidization flux fails to contribute to a positive bias flux, instead spilling over directly into the overflow. This result is surprising. However, the result is a simple extension of what happens when the gas flux imposed on the system is increased. As previously stated, at exceedingly low gas fluxes the imposed fluidization flux travels downwards creating positive bias. The volume fraction of gas in the foam, θ_0 , is determined by the fluidization flux and matches the volume fraction of gas in the overflow, θ_{OF} . But at higher gas flux, there is increased liquid that must report to overflow at steady state, and hence there is less positive bias flux. At even higher gas flux, there is eventually no bias flux, and hence the overflow liquid flux equals the fluidization flux. As the gas flux increases further even more liquid must report to the overflow, resulting in a negative bias flux. Eventually this negative bias flux corresponds to the flux curve constrained upward liquid flux, j_f . At this point the internal system is identical to that observed in the absence of any fluidization. This means the fluidization flux reports directly to the overflow in accordance with Equation 33. Also the volume fraction of the bubbles is lower than the original value, θ_0 , and is equal to θ_b . This system, at this point, behaves as though there was no fluidization, as the fluidization reports directly to the overflow.

For this flux curve constrained system fluidized at the upper boundary, Galvin et al. (2012) have shown that the bias flux is,

$$j_b = V_t (1 - \theta_b)^{n-1} [\theta_b^2 n - \theta_b (n+1) + 1]. \quad (34)$$

Equation 34 is applicable for bed concentrations ranging from the minimum, $\theta_{min} = 2/(n+1)$ (Wallis, 1969), corresponding to the flooding condition which occurs at the inflexion, through to the maximum, θ_0 , given by Equation 25. The maximum volume fraction is determined by the fluidization flux. This volume fraction cannot be exceeded because of the fluidization.

Figure 7A shows the bias flux versus the gas flux and Figure 7B shows the volume fraction of bubbles versus the gas flux. Again the fluxes have been normalized by the terminal velocity, V_t . The findings are presented for each of the cases shown in Figure 2 based on $n = 2$, and $j_w/V_t = 0.025$. Case (a) arises when no wash water is used, and shows a negative bias flux at all gas fluxes. Here, the system is always flux curve constrained. Case (b) arises when wash water is introduced deep within the foam zone. Above the wash water injection the system remains flux curve constrained. Case (c) arises when the fluidization boundary condition is applied, and the system is unconstrained by the flux curve. Here the bias flux is initially positive, then decreases to zero at constant volume fraction, and then becomes negative. Case (d) follows directly from Case (c), and arises when the system becomes flux curve constrained. At this point the added wash water reports directly to the overflow and hence the bias flux curve converges into Case (a). Equations 27 and 34 describe the transition from Case (c) to Case (d), at which point, $\theta_b = \theta_0$. Setting the volume fraction equal to θ_0 while rearranging Equation 9, it follows that $n = \frac{j_g (1 - \theta_0)}{V_s \theta_0^2}$. Incorporating this expression for n into Equation 34 along with Equation 24, it is possible to produce Equation 27. The maximum gas flux is given by the gas flux registered on the vertical axis when a tangent is drawn to the point of inflexion on the flux curve, corresponding to $\theta_{min} = 0.67$ at $n = 2$.

This work shows there is an important, yet subtle, distinction between wash water added at the upper distributor in Figure 2d versus that which enters inside the foam in Figure 2b. Naturally the elevation at which the wash water is injected can be raised to eventually coincide with a position an infinitesimal distance below the actual boundary. This shift has no bearing on these theoretical findings because Drift Flux theory does not address the effects of vertical gradients and hence physical elevation. For example, Drift Flux theory predicts steady state bubble volume fractions that are invariant with elevation. Therefore this analysis demonstrates a theoretical conundrum where, over an infinitesimal distance, there is the potential for the wash water addition to either join the product overflow directly (Case (d)),

maintaining a negative bias, or establish a downwards, positive, bias (Case (b)). This is the first time that this theoretical distinction has been recognised in the literature.

Interestingly, there appears to be some uncertainty in the literature regarding the partitioning of the wash water between the lower foam and the overflow product. Indeed, simulations involving water addition above the free-surface have demonstrated a significant portion of the water added simply flows over the weir thereby failing to wash the gangue from the foam (Neethling and Cilliers, 2001; Neethling et al., 2000). We hypothesize, however, that water injection through our fluidized bed distributor will emerge as though it had been delivered a finite distance below the distributor. Physically, the jetting of the water requires a finite distance before a uniform superficial flow velocity is formed. Hence, one goal of this study is to investigate this hypothesis and the consequences for positive bias and desliming.

3. Experimental

A schematic representation of the Reflux Flotation Cell (RFC) used in the experiments is shown in Figure 1. The cross-sectional area of the vessel was 99.7 mm x 83.9 mm. Feed slurry was pumped through a 35.0 mm internal diameter downcomer which formed an annulus around a 25.4 mm diameter tube that incorporated a porous sparger, 300 mm in length. The downcomer was longer than the sparger tube. Hence, the sparger tube was extended at each end by regular tubing in order to increase the length of the annulus. The horizontal cross-sectional area of the RFC, excluding the downcomer, was 0.0072 m². This area was used in the flux calculations.

The air rate to the sparger was controlled using a rotameter. A slurry feed rate of 3 L/min was used in the experiments, sufficient to promote a relatively mono-size bubble distribution. The outlet of the downcomer was positioned 0.67 m below the distributor used to achieve the fluidization hence there was a vertical distance of 0.33 m between the downcomer outlet and the entrance to the inclined channels. The distributor used in the fluidization incorporated holes 1.5 mm in diameter. Foam was expelled from the cell via a narrow annulus external to the downcomer, then through a 25 mm internal diameter hose located above the fluidization water inlet. Beneath the 1.0 m long vertical fluidization zone, a system of parallel inclined channels was formed using seven 0.7 mm thick stainless steel plates, each 1 m long. An angle of inclination of 70° to the horizontal was used, with the perpendicular distance between the surfaces of neighbouring plates fixed at 9.3 mm.

Two series of continuous steady state experiments were conducted. In each series a surfactant was introduced into both the feed slurry and fluidization water at a concentration of 0.2 g/L. The first set of experiments, presented in Section 4.1, examined the hydrodynamics of the fluidized bubble suspension in the absence of any particles. The surfactant used here, cetyl trimethyl ammonium bromide (CTAB), produced a mean bubble diameter of 240 μm , which was determined by photographic measurement. The foam interface was set 0.55 m below the fluidization inlet, at an elevation above the downcomer outlet. Thus the gas bubbles emerging from the downcomer segregated in an upwards direction to join the foam zone. It is emphasized that in these initial experiments the fluidization rates were relatively low and, consequently, the inclined channels were not utilized. Two underflow pumps were operated simultaneously. One pump provided a high base-level flow rate, while the other provided higher precision. This approach allowed careful control of the product overflow rate. The average liquid fraction in the foam was measured over a 0.25 m interval using a Rosemount

pressure transducer. Care was taken to ensure that no bubbles entered the lines to the transducer.

The second series of experiments, presented in Section 4.2, involved the use of silica particles to simulate the entrainment of fine gangue particles. 400G Sibelco silica was wet sieved to between 5 and 22 μm using Nylon filter bags. This preparation, which involved removal of the 0 to 5 μm particles, ensured that full mass balance closure could be achieved, given recovery of the 0 - 5 μm particles by sedimentation is difficult. Secondly, the preparation ensured a size distribution sufficiently fine that the particles would split with the flow of liquid to the overflow and underflow. A silica feed slurry concentrate was prepared by pre-mixing in an ultrasonic bath before being added to a 5.5 L mixing tank. The tank was regularly topped up with more feed during the course of each experiment.

In this second series of experiments the surfactant, sodium dodecyl sulfate (SDS), was used in order to ensure the silica particles did not float. Both the feed slurry and wash water were again set at 0.2 g/L of the surfactant. The concentrated slurry was mixed with the SDS solution to make up the 3 L/min volumetric rate entering the downcomer. The mean bubble size was measured to be 340 μm , slightly larger in this series of experiments. Samples, collected from the overflow and the underflow, were dried in an oven to determine the silica content. Four samples of the overflow and underflow streams were taken to confirm steady state operation. For these desliming experiments the effect of the position of the interface was tested using two distinct locations, (i) above the downcomer at an average distance of 0.49 m beneath the fluidization wash water inlet, and (ii) within the inclined channels, well below the downcomer outlet.

4. Results and Discussion

4.1 Investigation of the Fluidization Boundary Condition

In this first series of experiments the surfactant, CTAB, was used in order to generate relatively fine and stable gas bubbles. The objective was to investigate the effect of fluidization water on the hydrodynamics of the foam/bubble suspension. The wash water was delivered to the RFC via a distributor at the upper system boundary. According to the earlier analysis in this paper, there is some uncertainty in how to interpret the fluidization boundary condition.

The RFC is effectively an inverted fluidized bed, hence the liquid overflow flux from this device should be controllable via the underflow discharge rate. This series of fluidization experiments was conducted by initially forming steady state foam, with its base located above the downcomer outlet. It is noted that a pump was used in this study in order to provide additional control of the foam zone. Hence as the fluidization rate was increased, the underflow pumping rate was accordingly increased. Thus the foam interface of the fluidized bed was maintained at an approximately fixed level above the downcomer outlet, well above the inlet of the inclined channels.

The overflow liquid flux, j_f , versus the gas flux, j_g , is shown in Figure 8 for a range of fluidization fluxes, j_w . When no fluidizing wash water was used ($j_w = 0$ cm/s) the liquid flux emerging as an overflow product increased almost linearly with increasing gas flux. The gas flux was increased until the location of the foam interface became too difficult to visually discern, almost to the onset of flooding. Note that flooding occurred at a relatively low gas flux of 0.35 cm/s due to the mean bubble diameter, d_b , being relatively small at 240 μm . This data set, which involved no fluidization, provided the liquid overflow flux targets. Figure 8

shows that as the fluidization water was increased from 0 to 0.13 cm/s, only very modest changes in the overflow liquid flux were indeed produced, for a given gas flux. Clearly the underflow liquid flux was increased in direct response to the increase in the fluidization flux.

The smooth curve in Figure 8 was produced using Drift Flux theory, with $V_t = 2.7$ cm/s and $n = 3.2$. These fitted parameters insured reasonable agreement between the overflow liquid flux, j_f , and the gas flux, j_g , in the absence of any fluidization wash water. These fitted parameters were also used in the subsequent application of the Drift Flux theory to the other data sets in this section.

The implication of preserving the overflow flux to a level similar to that produced in the absence of fluidization is demonstrated in Figure 9. In this figure the bias flux, j_b , is plotted over a broad range of gas fluxes. By definition, when no fluidization is used, the bias flux is negative for all gas fluxes. For the fluidization flux, $j_w = 0.13$ cm/s, the bias flux shifted towards a positive bias over the entire range of gas fluxes examined. In effect, by preserving the overflow liquid flux at the non-fluidized level, the bias flux is directly adjusted by the amount of fluidization applied. The smooth curves are based on Drift Flux theory with $V_t = 2.7$ cm/s and $n = 3.2$. In the application of the theory it was further assumed that the fluidization wash water was applied beneath the upper system boundary. Hence, Figure 7 shows that the fluidization produces a result consistent with deep foam washing.

The relationship between the overflow liquid flux and the volume fraction of bubbles in the fluidized bed, with increasing gas flux, is shown in Figure 10A. The results are also shown in Figure 10B in terms of the volume fraction of the bubbles versus the gas flux. The experimental data shows that the volume fraction of the bubbles decreased significantly in response to a change in the fluidization flux from $j_w = 0$ to 0.13 cm/s. The agreement with the

theoretical result is reasonable in qualitative terms, but poor in numerical terms. The smooth curves were again produced using Drift Flux theory with $V_t = 2.7$ cm/s and $n = 3.2$. Drift Flux theory is conceptually powerful, but limited in its accuracy due to the range of simplifying assumptions. It is also possible that some error of significance arose in the measurement of the volume fraction via the pressure transducer measurements at the wall. In applying Drift Flux theory, it was assumed that the fluidization wash water was in effect delivered into the foam and hence the theoretical volume fractions correspond to the values calculated for the zone below the wash water injection, in accordance with Equation 23.

Typically, a foam will range from extremely “dry”, where the volume fraction of the bubbles approaches 1, to extremely “wet” randomly close-packed spheres with a volume fraction of about 0.74 (Fuerstenau et al., 2007; Weaire and Hutzler, 1999). When wash water is applied deep below the free-surface, bubble volume fractions of 0.60 have been reported without flooding (Ireland and Jameson, 2007). Here, bubble volume fractions as low as 0.45 were achieved. This low volume fraction of bubbles corresponds to significant permeability (Lorenceanu et al., 2009; Rouyer et al., 2010).

4.2 Desliming of Fine Silica from Flotation Foam

Ultrafine silica particles were used as a model system to assess the potential of the fluidization in desliming. It is noted that the surfactant, SDS, was used instead of CTAB in this series of experiments in order to ensure that the silica particles did not float. The bubbles observed were clearly coarser and found to have a mean size of 340 μm in diameter. Note the mean diameters in this study were calculated using the ratio $d_b = \sum D_i^3 / \sum D_i^2$, thus insuring the value could be related directly to both the gas flux and bubble surface flux. Hence the bubble surface flux becomes, $S_b = 6j_g/d_b$.

Initially, dilute silica slurry with a pulp density of 1.60 ± 0.14 % solids was fed into the RFC. The entrainment of silica, calculated in terms of its yield in the overflow, is shown in Figure 11 as a function of the gas flux, for different fluidization fluxes. The “wet” foam was operated within the vertical height of the downcomer, and hence the system of inclined channels played no role here. The applied fluidization fluxes were relatively low compared to those applied later in the study. Clearly, in the absence of any fluidization there was a direct increase in the silica entrainment with increasing gas flux. This increase is similar to the theoretical result that is also shown, based on the increasing water split to the overflow that arises as the gas flux increases. The modest divergence is attributed to the plume effect associated with the density of the incoming feed, which provides a degree of disengagement from the upward convective flow. With the addition of the fluidization water, however, the silica entrainment is shown to be substantially reduced, with the greatest relative reduction obtained for $j_g = 0.49$ cm/s and $j_w = 0.13$ cm/s.

Figure 12 shows the overflow liquid fluxes, j_f , versus the fluidization fluxes, j_w , for the intermediate and high gas flux. Here the system was either close to or beyond the flooding limit and hence the “wet” foam approached the conditions of a concentrated bubbly zone. The filled symbols denote the circumstances in which the concentrated bubbly zone extended into the system of inclined channels. Conversely the open symbols involved a “wet” foam that did not reach the system of inclined channels. These results show that the liquid flux reporting to the overflow can be preserved over a significant range of fluidization water fluxes. Note that for the two shaded squares in Figure 12 the fluidized bed occupied the entire length of the inclined channels, with the bubbles on the verge of reporting to the underflow. Here, the highest gas flux was 0.82 cm/s. Excess liquid, and hence entrained silica, was permitted to flow to the overflow in order to prevent bubbles escaping to the tailings stream.

Despite the small size of the bubbles ($d_b = 340 \mu\text{m}$), it was possible to operate at an extremely high wash water flux of 2.65 cm/s. For gas fluxes of 0.49 cm/s and 0.82 cm/s the bubble surface area flux, $S_b = 6j_g/d_b$, was 86 and 144 $\text{m}^2/\text{m}^2\text{s}$ respectively. These conditions are remarkable given that typical commercial flotation columns, with much larger bubbles of 1 to 1.5 mm in diameter, tend to operate with a wash water flux between 0.2 to 0.5 cm/s, at a gas flux within the limits of 0.6 to 2.0 cm/s.

The theoretical gas flux limit of a conventional system operated in the absence of wash water fluidization occurs at the flooding condition, which is obtained when the tangent of the operating line occurs at the point of inflexion. The relevant volume fraction at the inflexion point is $\theta_b = 2/(n+1)$. Equation 9 can be used to obtain the gas flux, j_g . In the present system $n = 3.2$, hence $\theta_b = 0.48$. Further, $V_t = 2.7 \text{ cm/s}$, and hence $V_s = 0.34 \text{ cm/s}$, and based on Equation 9, $j_g = 0.47 \text{ cm/s}$. The average bubble diameter is $d_b = 0.340 \text{ mm}$, thus the maximum bubble surface flux, $S_b = 6 \times 0.47 / 0.0340 = 83 \text{ s}^{-1}$. This result is consistent with the reported limit in the bubble surface flux of $S_b = 50 \text{ to } 100 \text{ s}^{-1}$ (Fuerstenau et al., 2007; Yianatos et al., 1987; Yianatos and Henríquez, 2007), depending on the bubble size. Typical operating levels in conventional cells reach $S_b = 30 \text{ to } 60 \text{ s}^{-1}$ (Massinaei et al., 2009). The extreme performance achieved in this study was due to the enhanced bubble-liquid segregation arising from the system of inclined channels. As a bubble descended into a channel it would rise and ascend along the upper surface of the channel, back to the fluidized bed above. This refluxing action occurred over a longer section of the inclined channels when higher fluidization water rates were employed.

Figure 13 shows the entrainment of silica, expressed as a yield %, versus the downwards liquid flux through the concentrated bubbly zone, the so-called bias flux. Once again, the

filled symbols denote conditions involving the concentrated bubbly zone within the system of inclined channels, while the unfilled symbols correspond to a “wet” foam zone that did not extend into the channels. A silica entrainment yield of 5.1 % was obtained using the lower gas flux, $j_g = 0.49$ cm/s, and no fluidization ($j_w = 0$ cm/s). However, by fluidizing the system at a water flux of $j_w = 0.13$ cm/s, there was a 4.6 fold reduction to 1.1 %. By increasing the fluidization to achieve a bias flux of 2.65 cm/s, the silica entrainment decreased by a further factor of 3 to 0.4%. Here the overflow concentration of silica was so low that its mass nearly equalled the mass of surfactant recovered in the product sample. For this sample, the actual entrainment of silica was measured by redissolving the SDS and decanting off the liquid. It is emphasized that great care was taken in obtaining all of the silica during the decanting, made possible by using a silica feed larger than 5 microns in diameter. We suspect this result represents the physical limit of the desliming process. The residual silica may be due to strong lubrication forces between the particles and the bubbles, arising from the high shear rate within the downcomer.

The dash line included in Figure 13 illustrates the trend anticipated from inclined channels configured to tolerate a higher downward liquid flux. It is also noted that the two shaded squares coincide with the condition referred to above of bubbles flooding the entire inclined channel zone. Here it is necessary to reduce the underflow rate to prevent the entrainment of bubbles into the tailings, which leads to excess liquid and hence silica reporting to the overflow.

Additional experiments were conducted using a higher feed pulp density of 6.5 ± 0.2 % solids. Figure 14 shows the overall liquid flux, 0.05 cm/s, is virtually independent of the fluidization flux up to about 1.15 cm/s. Beyond this limit the capacity of the inclined channel

system was exceeded, requiring a significant increase in the overflow liquid flux to 0.14 cm/s in order to prevent the losses of bubbles into the tailings. When the feed pulp density was lower at 1.6 % solids this limit was reached at a fluidization flux of 2.65 cm/s. Clearly, the higher pulp density led to a degree of hindered settling, reducing the segregation rate of the bubbles, and in turn the fluidization rate that could be applied. We suspect that the silica particles are associated strongly with the bubbles, in a purely hydrodynamic sense, due to the high shear rate in the downcomer. With such a high gas flux, that change in the level of the silica may have been significant with respect to the limited void space around the bubbles. It is known that the volume fraction of particles can influence the effective viscosity, so perhaps the high effective volume fraction led to a reduction in the bubble settling velocity.

Figure 15 provides some very interesting data on the silica entrainment obtained when the feed pulp density was 6.5 % solids. Two cases are presented. The first, represented by the dash curve, involved the use of foam. As noted previously, the foam was gradually lowered by increasing the tailings rate, until it entered the inclined channels. Given that foam lacks permeability, making the desliming process less efficient, the entrainment of silica was relatively high. However, in the second case, the base of the foam was permitted to rise up and out of the system by reducing the tailings rate. Hence the system was operated in an unconstrained manner, via a highly permeable bubbly zone, with only a slight increase in the liquid overflow liquid flux, as is shown in Figure 14. Then, by increasing the fluidization flux and by increasing the tailings rate to compensate for the additional liquid, the bubbly zone shifted downwards and into the system of inclined channels, delivering a concentrated bubbly zone. It is clear that the level of silica entrainment was nearly halved by choosing to operate without foam, and in turn operate with a highly permeable bubbly zone. It is also noted that a higher bias flux was achievable using the more permeable system. It should be noted that

under these conditions the volume fraction of the bubbles in the RFC was of order 0.5, substantially higher than the typical level of 0.05 to 0.15 in the dilute bubbly zone of mechanical cells (Fuerstenau et al., 2007).

5. Concluding Remarks

The Reflux Flotation Cell (RFC) is designed to overcome the inherent hydrodynamic constraints of conventional flotation cells. Drift Flux and fluidization theory were used to investigate the fluidization boundary condition of the system. The experimental results showed that the fluidization wash water was, in effect, delivered into the foam or concentrated bubbly zone via the distributor. Hence the fluidization wash water was permitted to travel downwards delivering significant positive bias and hence strong desliming of the flotation foam.

The hydrodynamics of the Reflux Flotation Cell led to remarkably high bubble surface area fluxes of order $144 \text{ m}^2/\text{m}^2\text{s}$, well in excess of the theoretical limit of a conventional system. The fluidization water permeated downwards through the bed of rising bubbles. The inclusion of multiple parallel inclined channels beneath the fluidized bed provided an enhanced rate of segregation between the rising bubbles and descending liquid, allowing extremely high fluidization fluxes and hence bias fluxes to be applied.

Silica was used as a model hydrophilic particle species in order to investigate the hydrodynamic benefits of the RFC configuration in desliming. In general the best performance was achieved by choosing to operate with a concentrated bubbly zone rather

than foam. This bubbly zone had a lower volume fraction of bubbles in the vicinity of 0.5. The increased permeability proved ideal for efficient desliming at high wash water fluxes.

6. Disclosure Statement

The University of Newcastle holds international patents and patent applications on the Reflux Classifier and related technologies and has a Research and Development Agreement with FLSmidth Ludowici to develop these technologies.

7. Acknowledgements

The authors acknowledge the financial support of the Australian Research Council and the Australian Coal Association Research Program, as well as the on-going support of FLSmidth Ludowici in supporting this work.

8. References

- Boycott, A.E., 1920. Sedimentation of blood corpuscles. *Nature* 104, 532.
- Finch, J.A., Dobby, G.S., 1990. *Column Flotation*. Pergamon Press, New York.
- Fitch, B., 1979. Sedimentation of flocculent suspensions: state of the art. *AIChEJ.* 25(6), 913-930.
- Fuerstenau, M.C., Jameson, G.J., Yoon, R.H., 2007. *Froth Flotation: A Century of Innovation*. SME.
- Galvin, K.P., and Dickinson, 2013. Fluidized Bed Desliming in Fine Particle Flotation – Part II Flotation of a Model Feed, *Chemical Engineering Science*, under review.
- Galvin, K.P., Zhou, J., Dickinson, J.E., Ramadhani, H., 2012. Desliming of dense minerals in fluidized beds. *Minerals Engineering* 39, 9-18.

- Galvin, K.P., Zhou, J., Walton, K., 2010. Application of closely spaced inclined channels in gravity separation of fine particles. *Minerals Engineering* 23, 326-338.
- Grassia, P., Neethling, S.J., Cilliers, J.J., 2002. Foam drainage on a sloping weir. *The European Physical Journal E: Soft Matter and Biological Physics* 8, 517-529.
- Ireland, P.M., Jameson, G.J., 2007. Liquid transport in a multi-layer froth. *Journal of Colloid and Interface Science* 314, 207-213.
- Kynch, G.J., 1952. A theory of sedimentation. *Transactions of the Faraday Society* 48, 166-182.
- Lorenceanu, E., Louvet, N., Rouyer, F., Pitois, O., 2009. Permeability of aqueous foams. *European Physical Journal E* 28, 293-304.
- Massinaei, M., Kolahdoozan, M., Noaparast, M., Oliazadeh, M., Yianatos, J., Shamsadini, R., Yarahmadi, M., 2009. Hydrodynamic and kinetic characterization of industrial columns in rougher circuit. *Minerals Engineering* 22, 357-365.
- Nakamura, H., Kuroda, K., 1937. La cause de l'accélération de la vitesse de sédimentation des suspensions dans les récipients inclinés. *Keijo J. Med.* 8, 256-296.
- Neethling, S.J., Cilliers, J.J., 2001. Simulation of the effect of froth washing on flotation performance. *Chemical Engineering Science* 56, 6303-6311.
- Neethling, S.J., Cilliers, J.J., Woodburn, E.T., 2000. Prediction of the water distribution in a flowing foam. *Chemical Engineering Science* 55, 4021-4028.
- Ponder, P., 1925. On sedimentation and rouleaux formation. *Quart. J. Exp. Physiol.* 15, 235-252.
- Richardson, J.F., Zaki, W.N., 1954. Sedimentation and fluidisation: Part I. *Trans IChemE* 32, 34-53.
- Rouyer, F., Pitois, O., Lorenceanu, E., Louvet, N., 2010. Permeability of a bubble assembly: From the very dry to the wet limit. *Physics of Fluids* 22, 1-5.

- Stevenson, P., Mantle, M.D., Sederman, A.J., Gladden, L.F., 2007. Quantitative measurements of liquid holdup and drainage in foam using NMRI. *AIChE Journal* 53, 290-296.
- Wace, P.F., Alder, P.J., Banfield, D.L., 1968. Foam separation process design. Internal Report, Atomic Energy Research Establishment, Harwell, Oxfordshire, Harwell HL68/5699.
- Wallis, G.B., 1969. One-dimensional two-phase flow. McGraw-Hill, New York.
- Weaire, D., Hutzler, S., 1999. The physics of foam. Oxford University Press, Oxford.
- Yianatos, J.B., Finch, J.A., Laplante, A.R., 1987. Cleaning action in column flotation froths. *Trans. Inst. Min. Metall. C*, C199-C205.
- Yianatos, J.B., Henríquez, F., 2007. Boundary conditions for gas rate and bubble size at the pulp-froth interface in flotation equipment. *Minerals Engineering* 20, 625-628.
- Zhou, Z.A., Egiebor, N.O., 1993. Technical note. A gas-liquid drift-flux model for flotation columns. *Minerals Engineering* 6, 199-205.

Appendix A

In this Appendix the analogous system of a steady state thickener is outlined with reference to the theory of Kynch (1952). Readers are also referred to the article “State of the Art” (Fitch, 1979). In this analogy we equate the individual solid particles which settle downwards with the individual gas bubbles that “settle” upwards in a system of rising foam. Figure A1 shows a schematic representation of the system, which is treated as a one dimensional process in the vertical direction, with a constant cross-sectional area.

A dispersed flux of solid particles, j_s , is introduced, resulting in a low concentration of particles settling downwards towards the base of the thickener of constant cross-sectional area. The theory of Kynch predicts the formation of concentration waves that rise upwards at a propagation velocity given by the slope of the flux curve. Note that the flux curve is formed from a plot of $V_s\theta$ versus θ , where V_s is the batch settling velocity as defined by Equation 1, and θ is the volume fraction of the dispersed phase. The slope of the flux curve is,

$$V_p = -\frac{d(V_s\theta)}{d\theta}. \quad (\text{A1})$$

The rise velocity of the sediment bed is determined by the maximum propagation velocity that can be sustained by the feed flux. Note that here V_p is numerically positive in the upwards direction while the settling velocity, V_s , is numerically positive in the downwards direction. We also assign the specific term, V_{pb} , to denote the rise velocity of the bed, the key focus of our analysis. We also assign the specific term, V_{sb} , to denote the settling velocity of the solids that are present just below the surface of the bed.

The volume fraction of solids just below the surface of the rising bed is θ_b . Higher concentrations are present at lower elevations within the bed, and clearly rise at propagation velocities lower in magnitude than the magnitude $|V_{pb}|$ at θ_b . When the underflow pump is finally applied at a sufficient velocity, $V_{UF} = |V_{pb}|$, the rise velocity of the bed, relative to the vessel, decreases to zero. Given that the magnitudes of the rise velocities of all other concentrations within the bed must be less than the original bed rise velocity magnitude, $|V_{pb}|$, and given that the underflow pump imposes a downwards velocity of magnitude, $|V_{pb}|$, these higher concentrations now propagate downwards and out of the system, leaving just one constant concentration within the bed, θ_b .

This pumping operation also results in a fixed interface position between the free-settling zone and sediment bed, and hence steady state. A small disturbance can easily lead to a rise or a fall in the bed level, so some effort is needed in order to keep the interface fixed. At this point the volume flux of solids, j_s , and the volume flux of liquid fluid, j_f , passing down through both the free settling zone and sediment bed are fixed and equal to the flux of solids and fluid emerging via the underflow. This volumetric underflow flux matches the magnitude of the original propagation velocity of the bed, $|V_{pb}|$. Therefore,

$$|V_{pb}| = j_s + j_f. \quad (\text{A2})$$

The above discussion is readily quantified using an appropriate flux curve construction. Although we normalize the flux curve using the particle terminal velocity, V_t , the normalization is neglected in the discussion to simplify the description. The settling flux of the solid particles is given by the product of the settling velocity, V_s , and volume fraction of solids, θ . The basis of this velocity, V_s , as applied to particles, is defined by Equation 1. We have chosen to normalize the flux curve with respect to the particle terminal velocity, V_t . We have also assumed a value for $n = 2$ in Equation 1, despite the fact that in practice the value will normally be larger. This lower value of n has been used because it provides a clearer illustration of the detailed flux curve construction. Figure A2 shows the flux curve produced using a plot of the settling flux of the solids, $V_s\theta$, versus the volume fraction of solids, θ . A Yoshioka flux curve construction (Fitch, 1979), consisting of an operating line extending from the imposed solids feed flux, j_s , on the vertical axis down to the flux curve, as a tangent, is shown.

The tangent occurs at the volume fraction, θ_b , which is the concentration just below the surface of the bed. Further, the slope of the tangent is the corresponding propagation velocity, V_{pb} , which is the rise velocity of the bed in the absence of any underflow removal. This is the

maximum propagation velocity that can be sustained by the feed flux, j_s , and hence this tangent condition governs the properties of the bed surface. In order to achieve steady state, an underflow flux, V_{UF} , is imposed equal in magnitude and opposite in direction to the propagation velocity, V_{pb} , of the bed. The tangent intersects the horizontal axis at the steady state underflow concentration, θ_{UF} . The slope of the chord from the origin to the point at which the tangent meets the flux curve is clearly V_{sb} . It therefore follows that,

$$j_s = (|V_{pb}| + V_{sb})\theta_b \quad (\text{A3})$$

and hence the imposed solids flux, j_s , establishes a propagation flux component, $|V_{pb}|\theta_b$ and settling flux component, $V_{sb}\theta_b$.

Figure A3 shows the alternative flux curve construction, based on a plot of the modified settling flux, $(V_{UF} + V_s)\theta$. Here the flux curve shows the total flux passing through the system, and hence the relevant operating line becomes horizontal, extending from j_s horizontally to the line defining the underflow velocity, intersecting at the underflow concentration. At θ_b the flux curve exhibits a “bottle-neck”, or minimum value equal to j_s . This feed flux, j_s , is the maximum that can be transported to the underflow at this underflow velocity. Clearly a higher feed flux will lead to accumulation within the system and hence a rising bed, and therefore failure to reach steady state. The system is therefore constrained by the flux curve when the feed flux is greater than or equal to j_s . However, a lower feed flux can be imposed, resulting in a proportionally lower underflow concentration, governed by material balance alone. Here the system is not constrained by the flux curve. While this construction provides a clearer picture of the flux constraints of the thickener, it is necessary to produce a new plot in order to represent the effect of each underflow velocity. Hence the Yoshioka construction is preferable, given its application for virtually any underflow velocity, yielding equivalent information.

- The Reflux Flotation Cell transforms the hydrodynamics of flotation
- A conundrum emerges when wash water addition is formally applied at the boundary
- Parallel inclined channels enhance bubble-liquid segregation rates
- Bubble surface fluxes in excess of the normal flooding limit can be used
- Desliming is enhanced via a highly permeable concentrated bubbly zone

Accepted manuscript

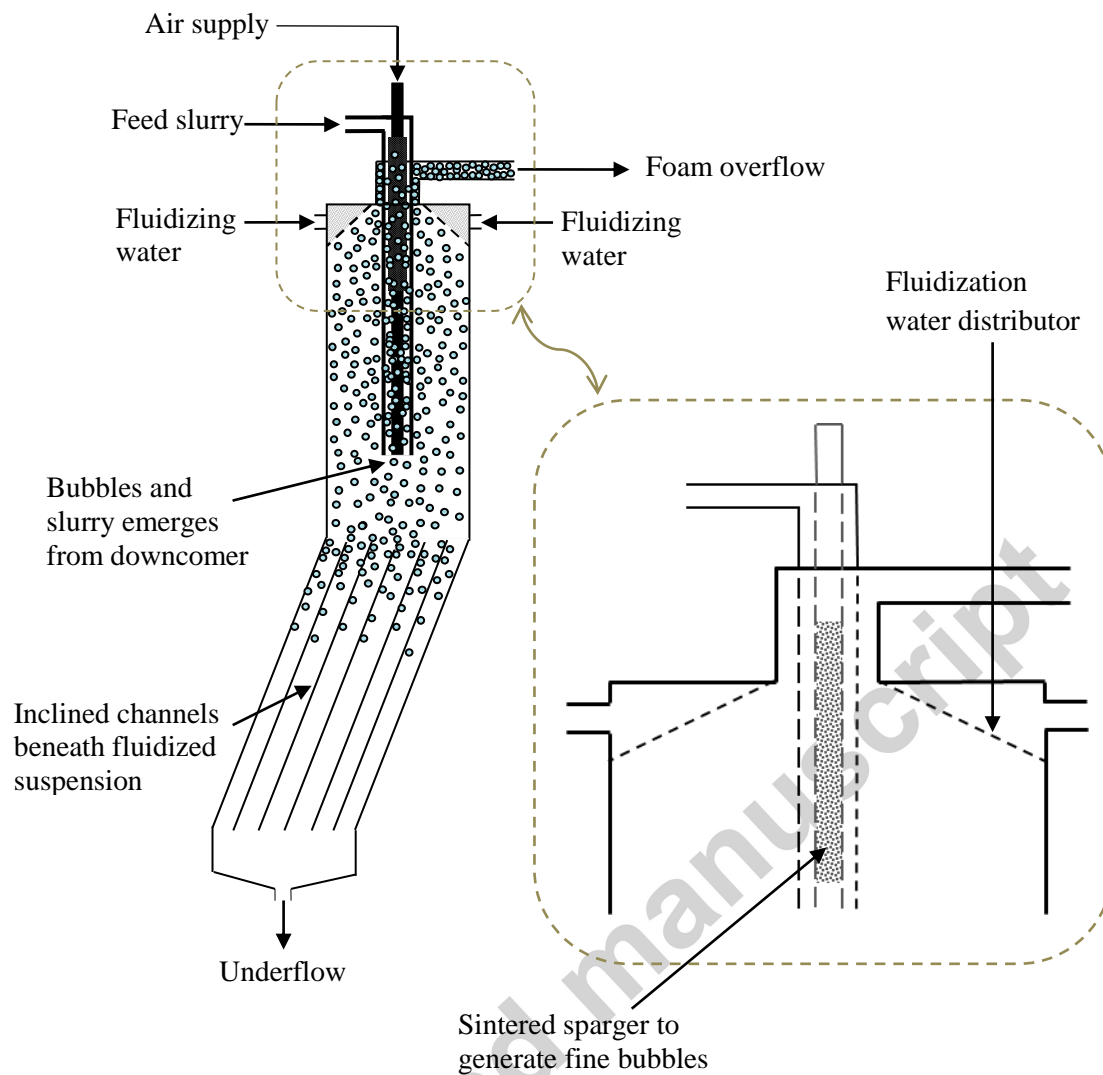


Figure 1: The Reflux Flotation Cell (RFC) with internal wash water fluidization. The fluidization distributor surrounds the entire top of the cell thus providing uniform washing, while permitting overflow discharge through a narrow port. Inclined channels enhance bubble-liquid segregation.

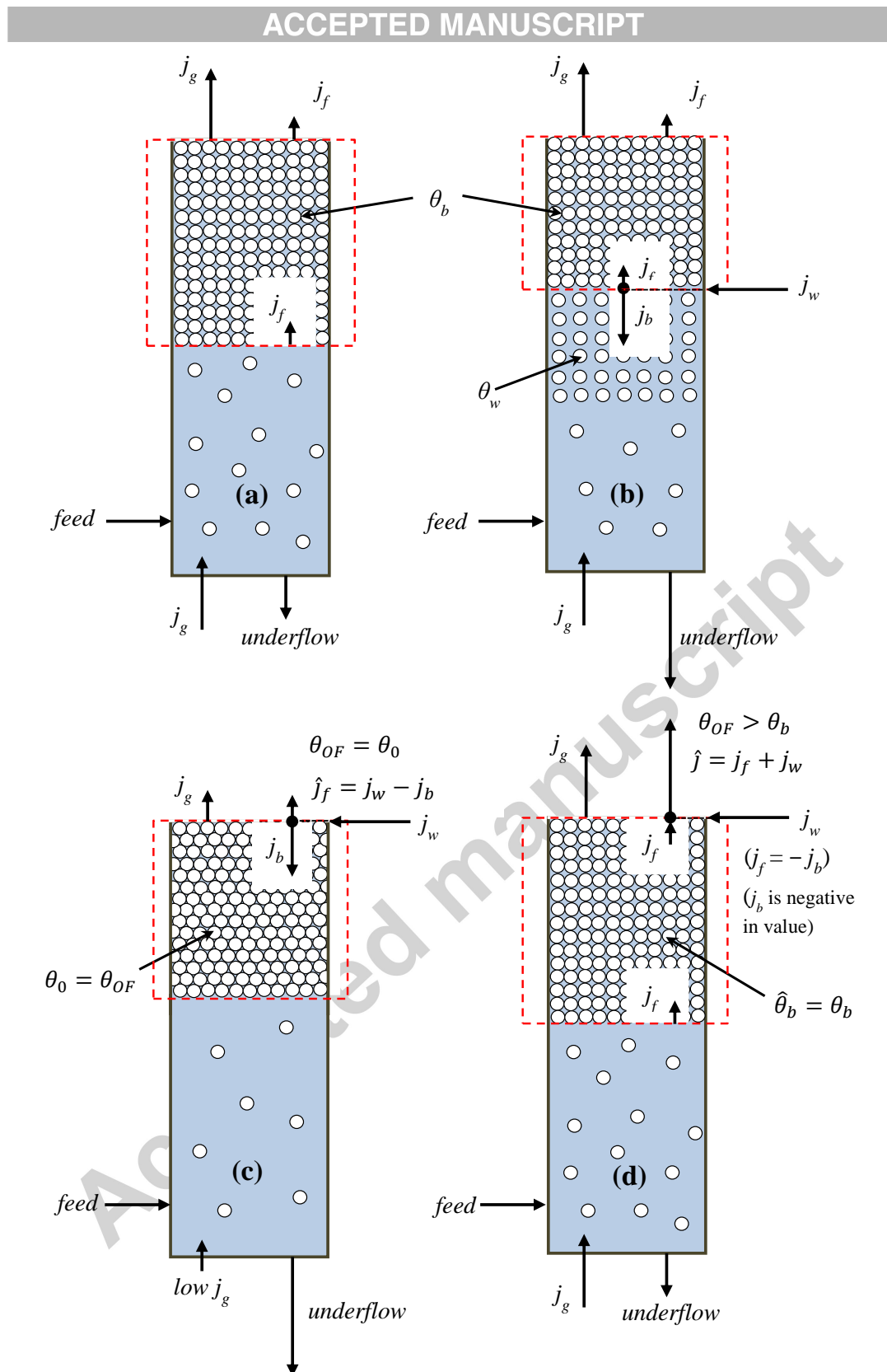


Figure 2: (a) Flotation with no wash water addition (constrained). (b) Wash water applied internally below the free-surface of the foam (constrained). (c) Fluidizing wash water applied externally at the free-surface boundary using a low gas flux (unconstrained). (d) Fluidizing wash water applied externally at the free-surface boundary using a high gas flux (constrained).

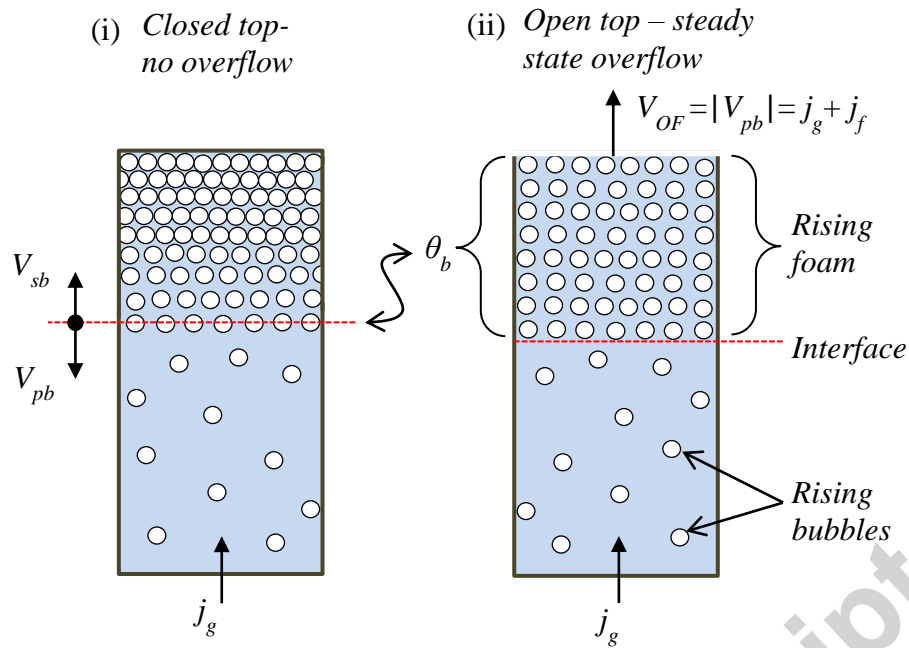


Figure 3A: (i) Batch “settling” of bubbles in vertical vessel with no overflow removal. The leading interface descends downwards at propagation velocity, V_{pb} , with bubble concentration θ_b . (ii) The foam-bubbly zone interface is made fixed by discharging the overflow at velocity $V_{OF} = |V_{pb}|$.

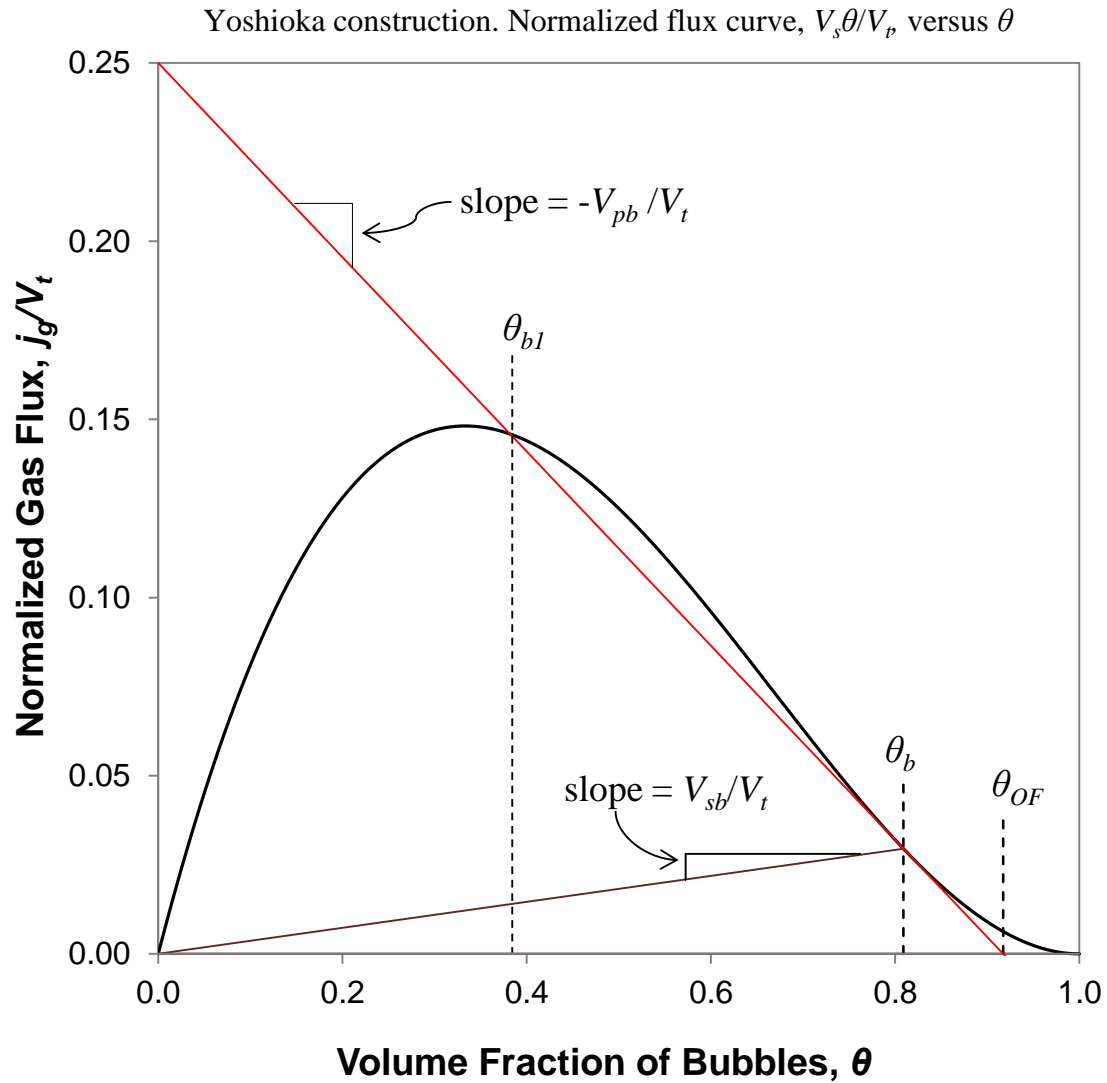


Figure 3B: Normalized flux curve showing $V_s\theta$ versus θ , with V_s based on Equation 1 with $n = 2$. The Yoshioka construction provides a description of both the batch and steady state system for a normalized gas flux, j_g/V_t . The operating line extends from the gas feed flux on the vertical axis ($j_g/V_t = 0.25$) to the flux curve as a tangent, and intersects the horizontal axis at the steady state overflow concentration, θ_{OF} . The normalized steady state overflow velocity, V_{OF}/V_t , equals the magnitude of the slope of the operating line.

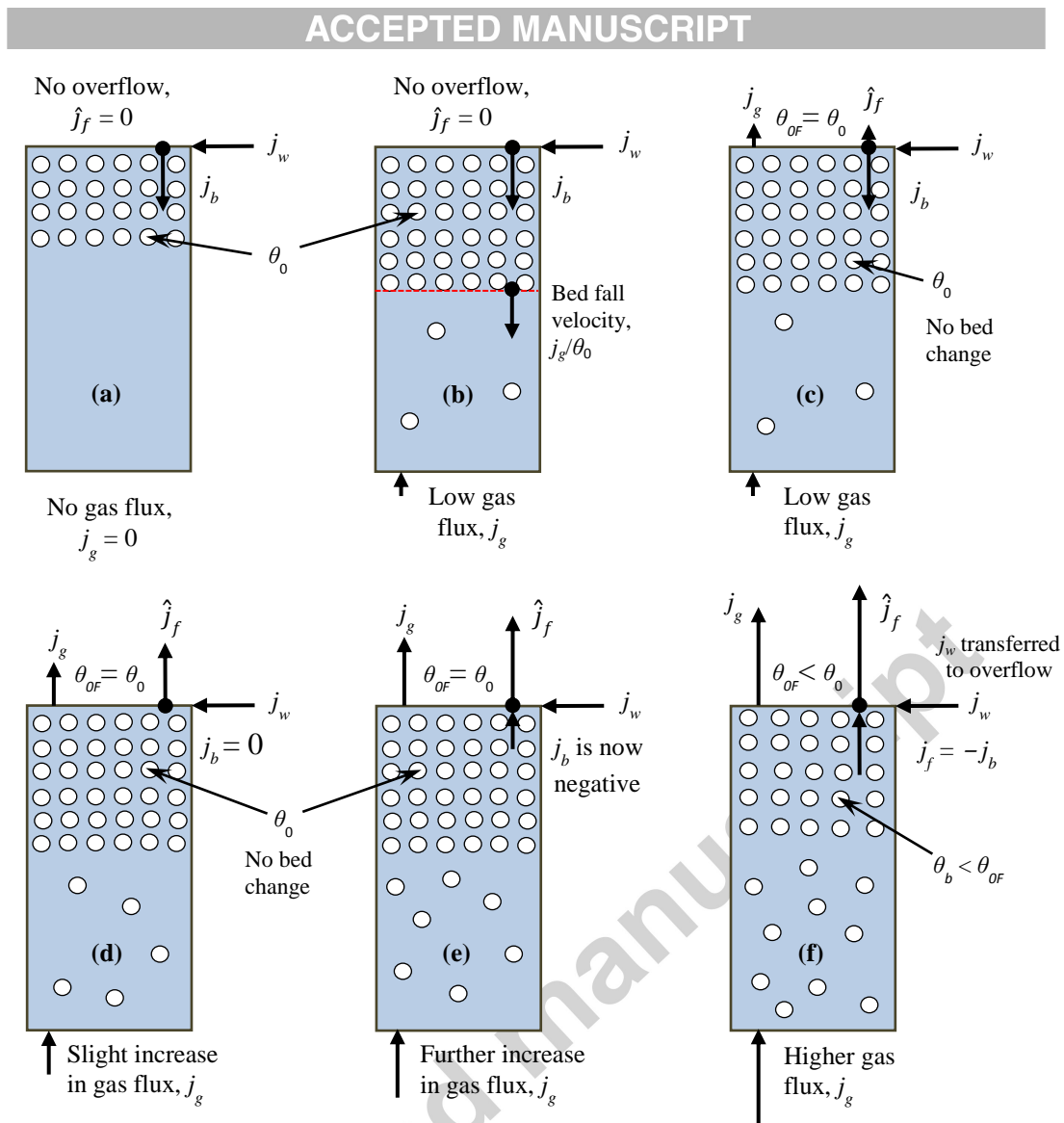


Figure 4: The effect of increasing gas flux on a fluidized bed of bubbles using a fixed fluidization flux, j_w . Operation (a) and (b) have no overflow, whereas (c) to (f) have overflow permitted. (a) has a fixed inventory of bubbles. (c), (d) and (e) are unconstrained by the flux curve, whereas (f) is flux curve constrained.

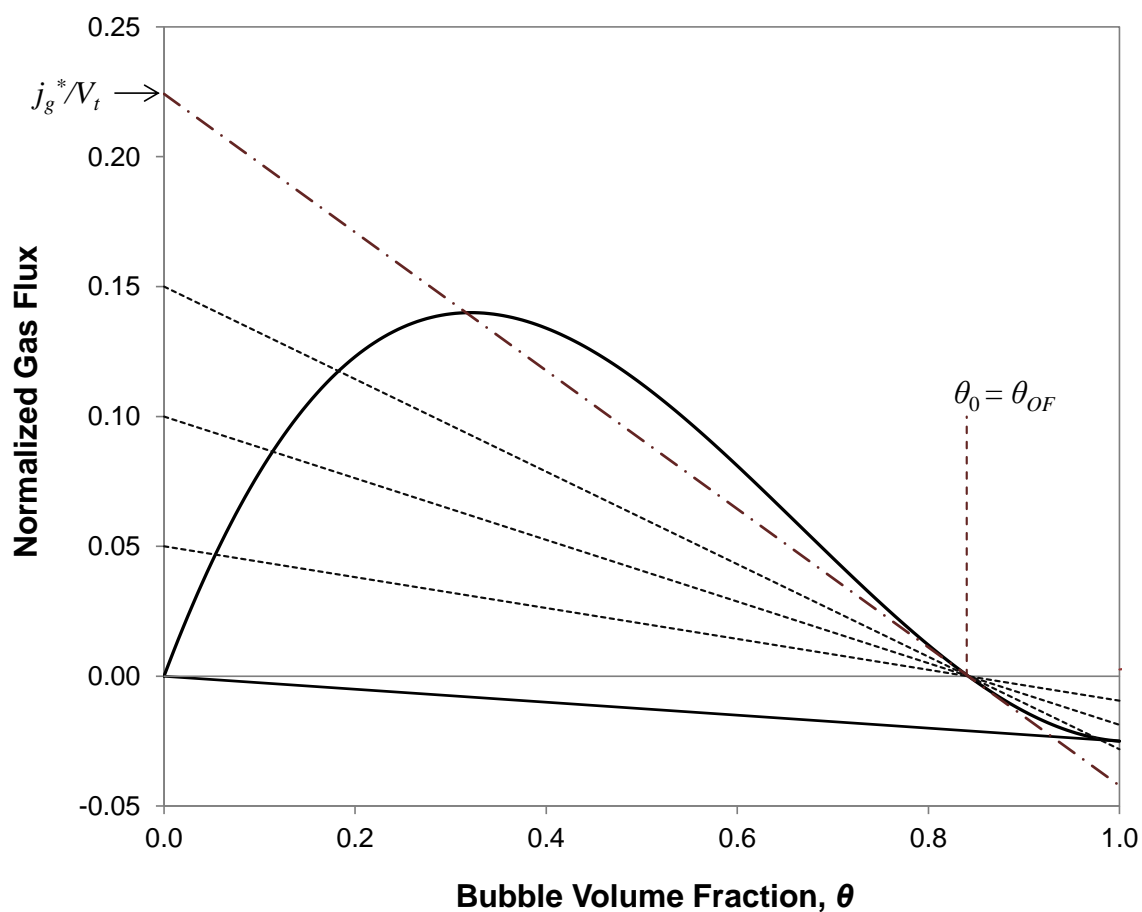


Figure 5: Operating lines unconstrained by the normalized flux curve with j_g/V_t decreasing from $j_g^*/V_t = 0.224$ down to $j_g/V_t = 0.05$. The value of $n = 2$ and the fluidization flux is $j_w/V_t = 0.025$. The slope of each operating line denotes the discharge flux of gas and liquid, analogous to the operation of a thickener.

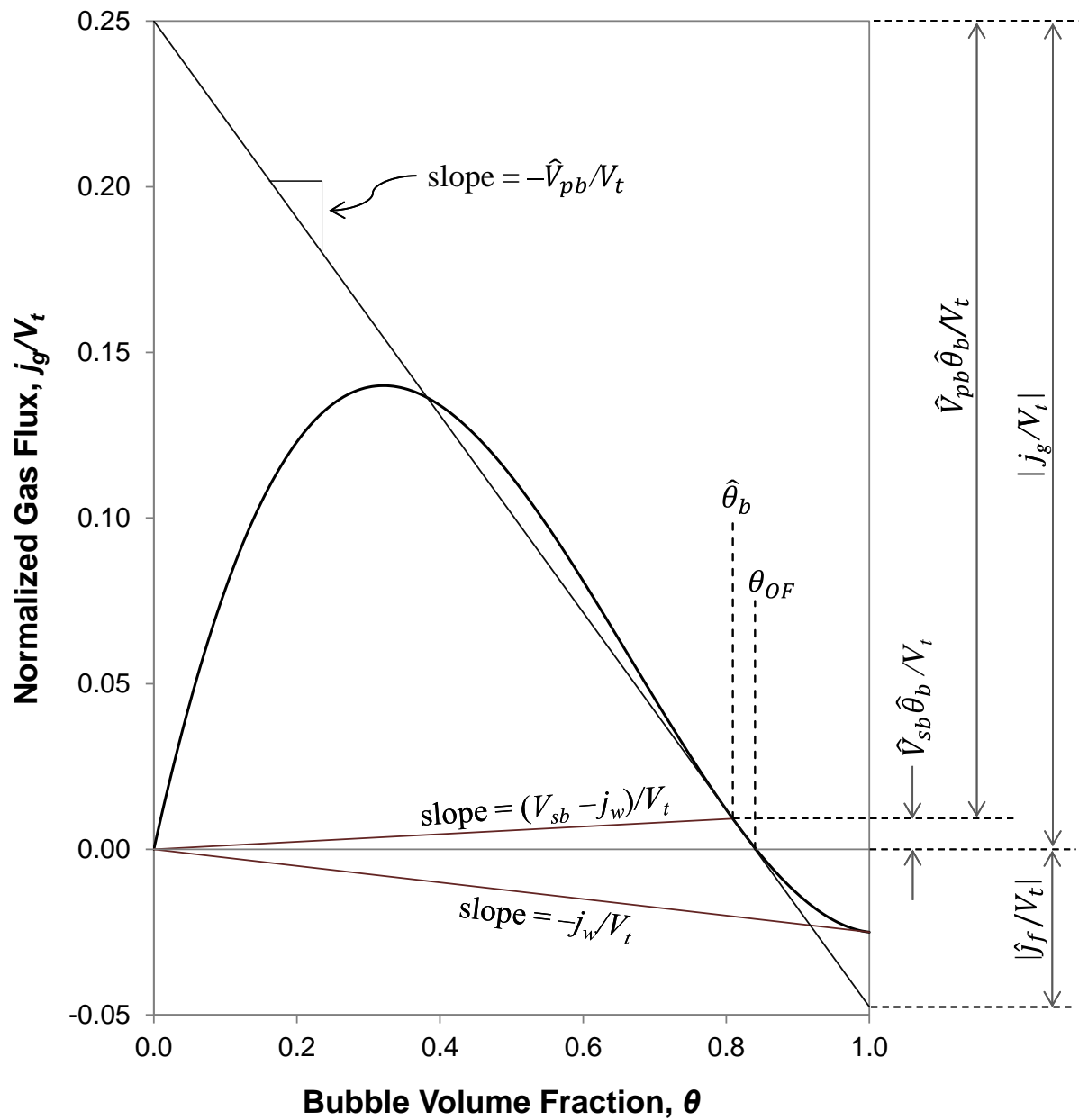


Figure 6: Flux curve constrained flotation with fluidizing wash water. Fluxes have been normalized by the bubble terminal velocity, V_t . Other parameters used are $n = 2$ and $j_w/V_t = 0.025$. The arrows shown above represent flux quantities that sum to produce the gas flux in accordance with Equation 32.

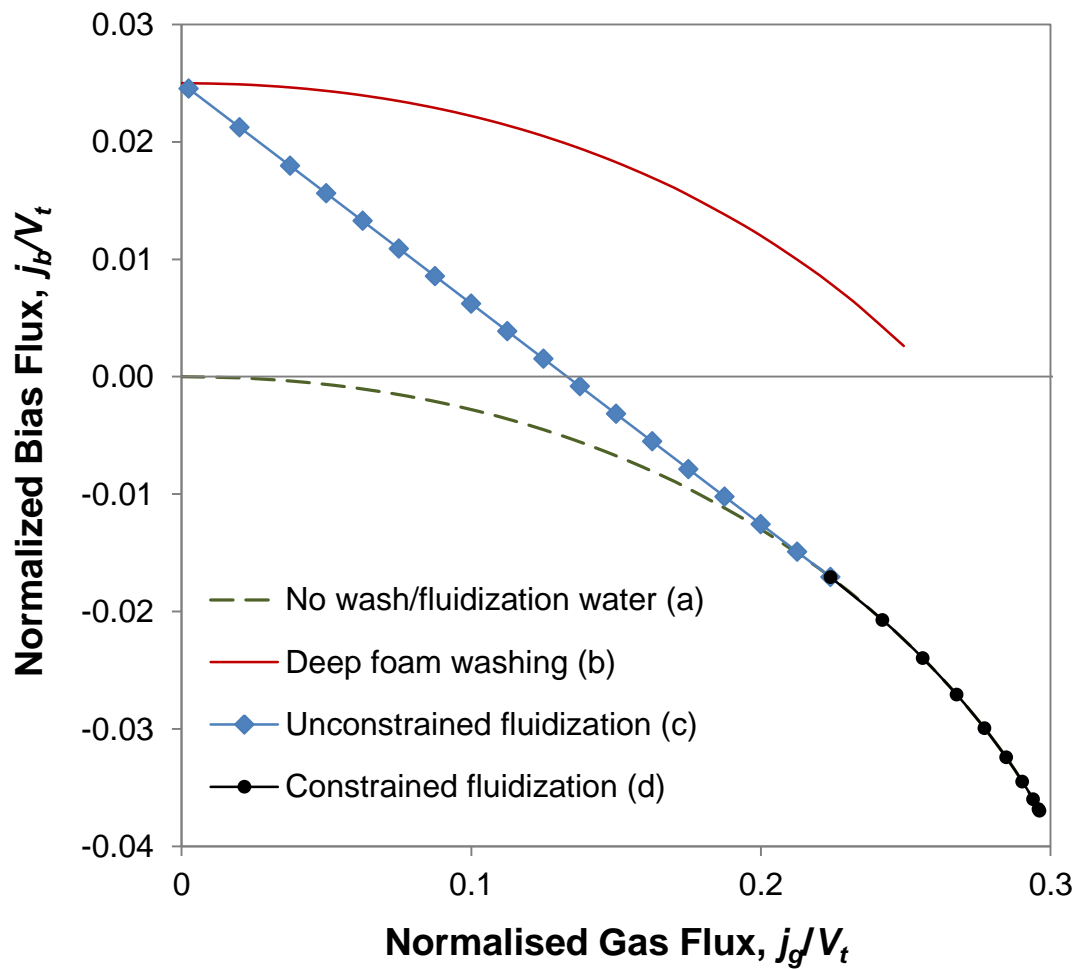


Figure 7A: The theoretical bias flux versus the gas flux for different fluidization/wash water boundary conditions, normalized by V_t . The relevant conditions from Figure (2) are denoted by the letters (a) to (d). The potential for desliming is increased when operating with a positive bias, which is shown to be more readily achievable at lower gas fluxes, but only for the unconstrained fluidization and deep foam washing cases. The fluidization flux is $j_w/V_t = 0.025$. Note that the maximum gas flux obtained using deep foam washing is lowered by the earlier onset of flooding (Galvin and Dickinson, 2013) and hence the covers a small range of gas fluxes.

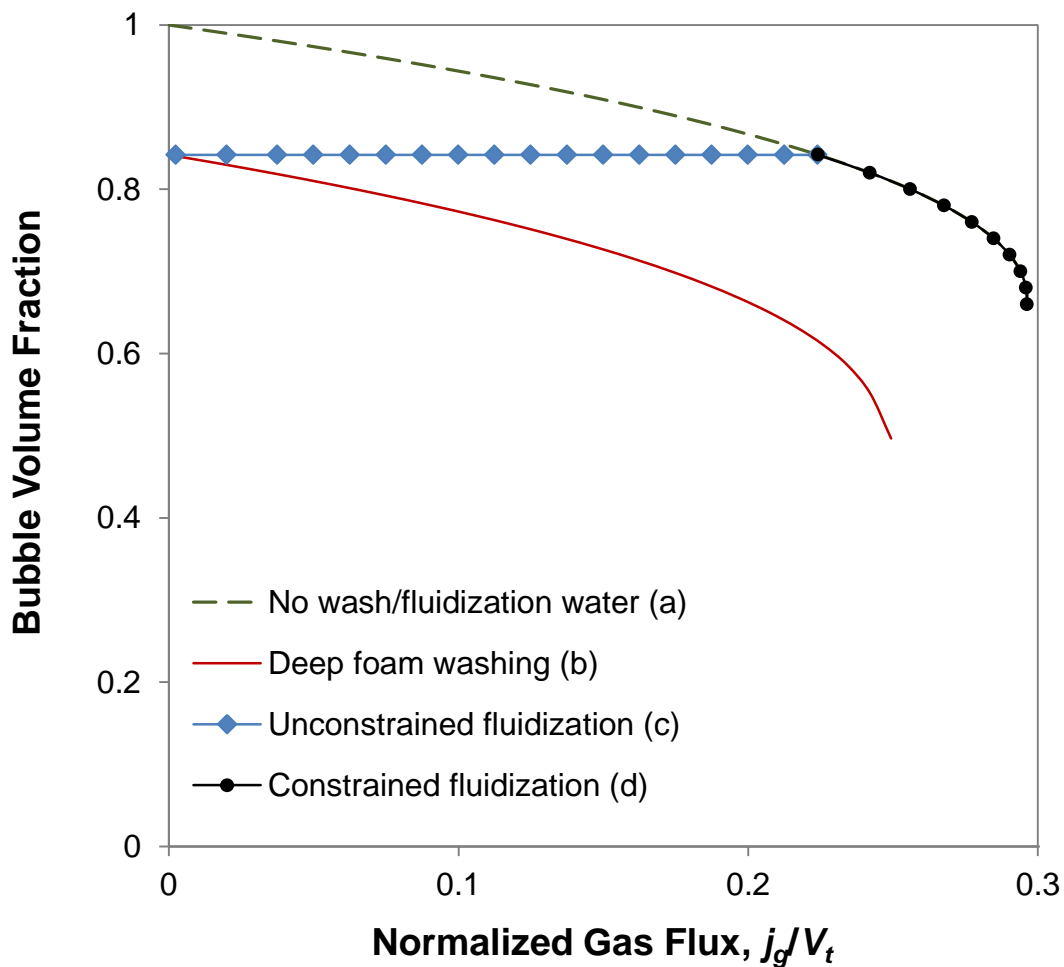


Figure 7B: The theoretical volume fraction of bubbles versus the normalized gas flux corresponding to the four fluidization/wash water boundary conditions presented in Figure 7A. The bubble volume fraction beneath the wash water boundary in deep foam washing is lowered by the downward transfer of water. Above the wash water injection boundary the foam zone has the same bubble volume fraction as the no wash/fluidization water result, for a given bubble size and gas flux. In case (c) the bubble volume fraction is independent of the gas flux prior to the flux curve constrained conditions of case (d). This constant volume fraction is consistent with the application of the fluidization boundary condition.

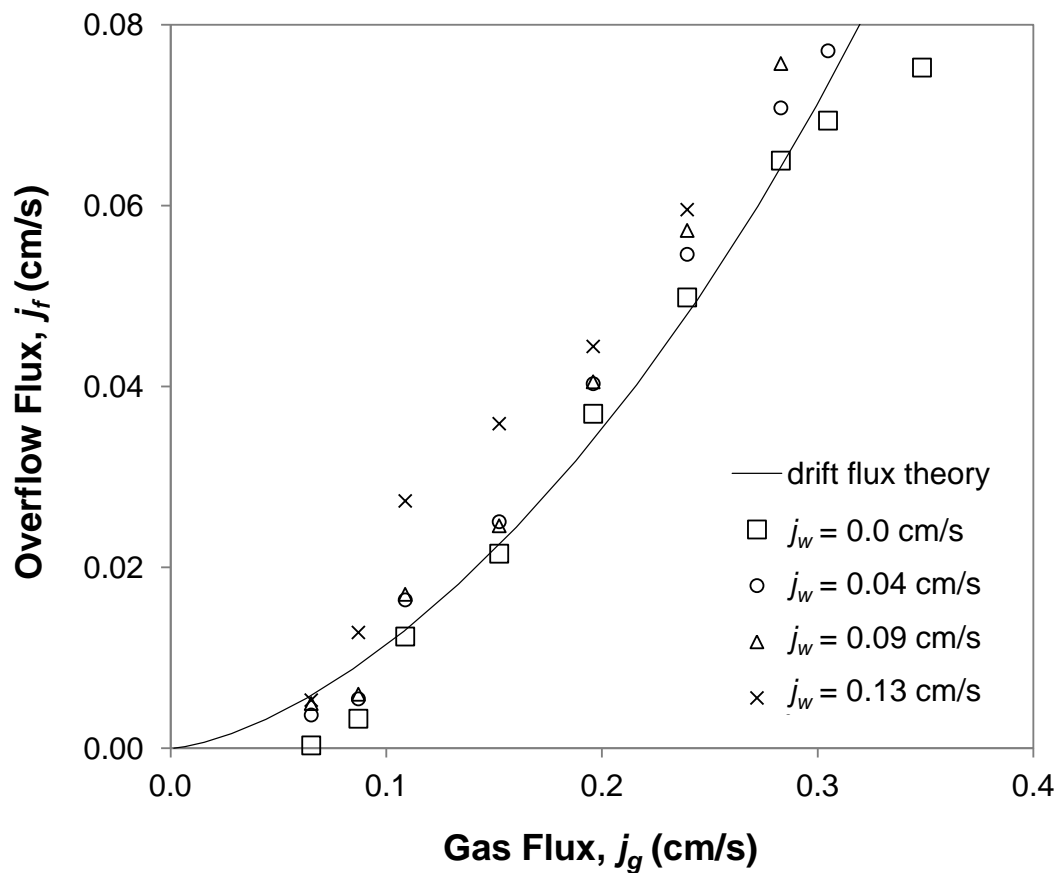


Figure 8: The liquid overflow flux versus the gas flux for a range of fluidization fluxes, with $j_w = 0$ to 0.13 cm/s. For a given gas and fluidization flux, the overflow flux can be maintained at the non-fluidization flux value by increasing the tailings discharge rate to account for the added fluidization water. The data corresponding to the case involving no fluidization were used to establish the Drift Flux theory parameters. In turn, the smooth curve shows j_f versus j_g based on $V_t = 2.7$ cm/s and $n = 3.2$.

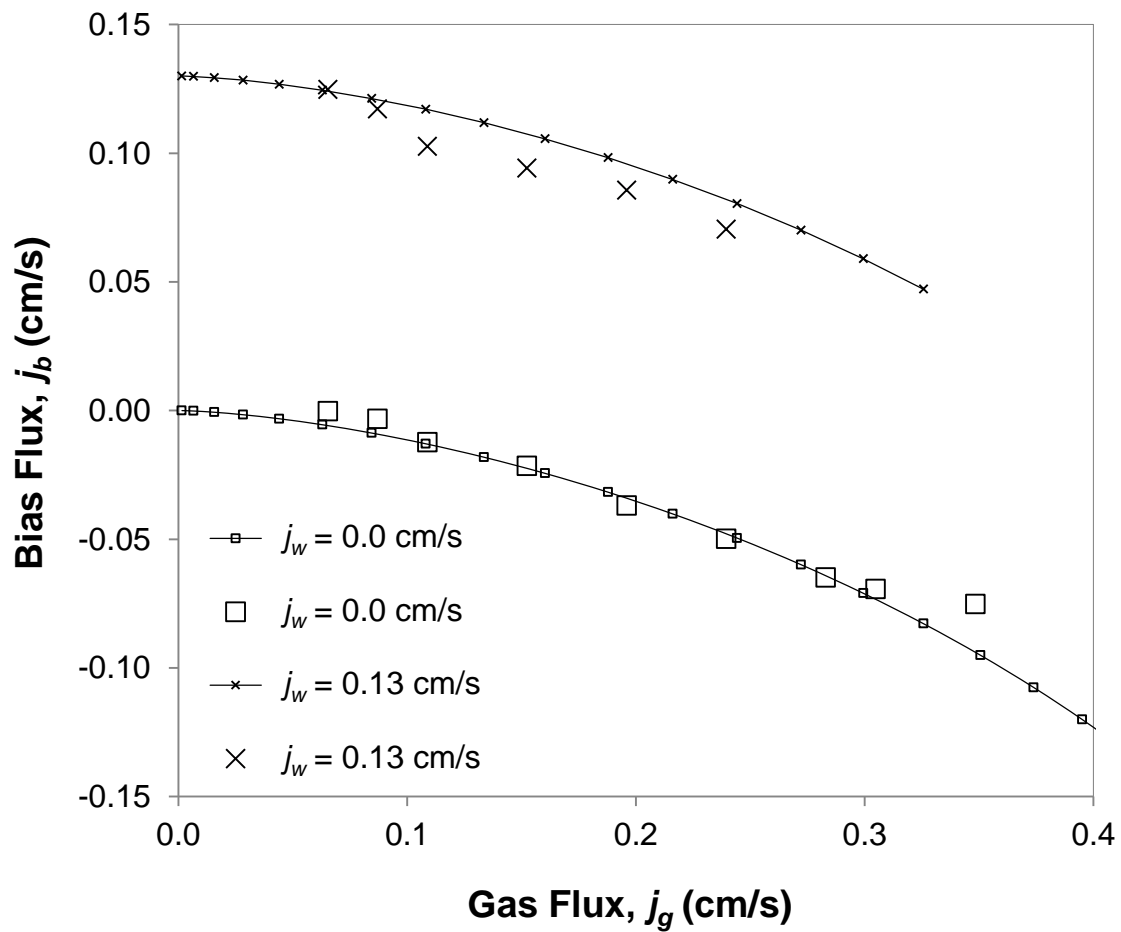


Figure 9: The bias flux versus the gas flux within the RFC with the fluidized foam positioned above the downcomer outlet. The curves through the data sets are based on Drift Flux theory, with $V_t = 2.7$ cm/s and $n = 3.2$. A strong positive bias is evident for the fluidization wash water flux $j_w = 0.13$ cm/s, while for the case involving no fluidization the bias flux is always negative.

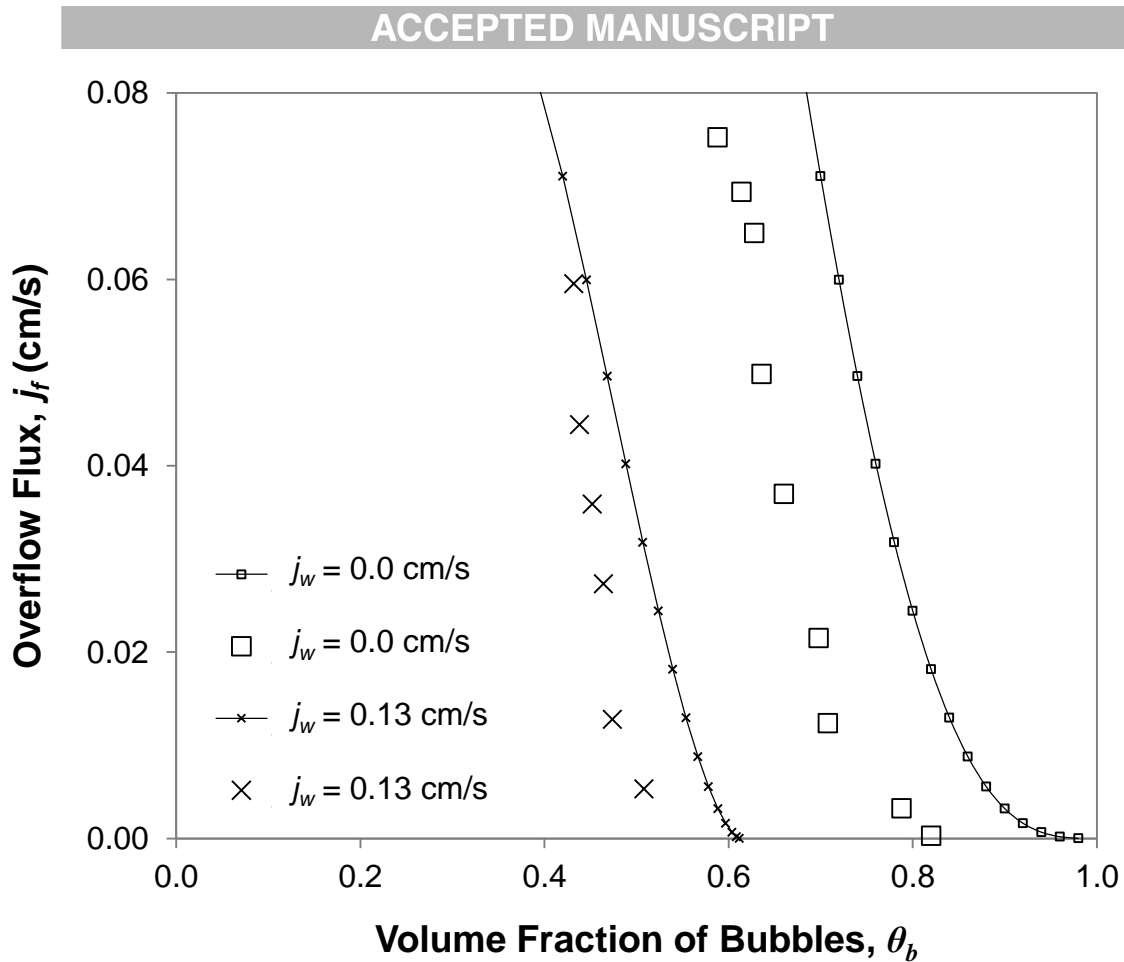


Figure 10A: The overflow flux is shown versus the volume fraction of the bubbles as determined using a pressure transducer. Here the fluidized bed was positioned above the downcomer outlet. The curves through the data sets are based on Drift Flux theory, with $V_t = 2.7$ cm/s and $n = 3.2$. Clearly, the volume fraction of the bubbles decreases significantly in response to the fluidization wash water. Some discrepancy between the model and data are evident.

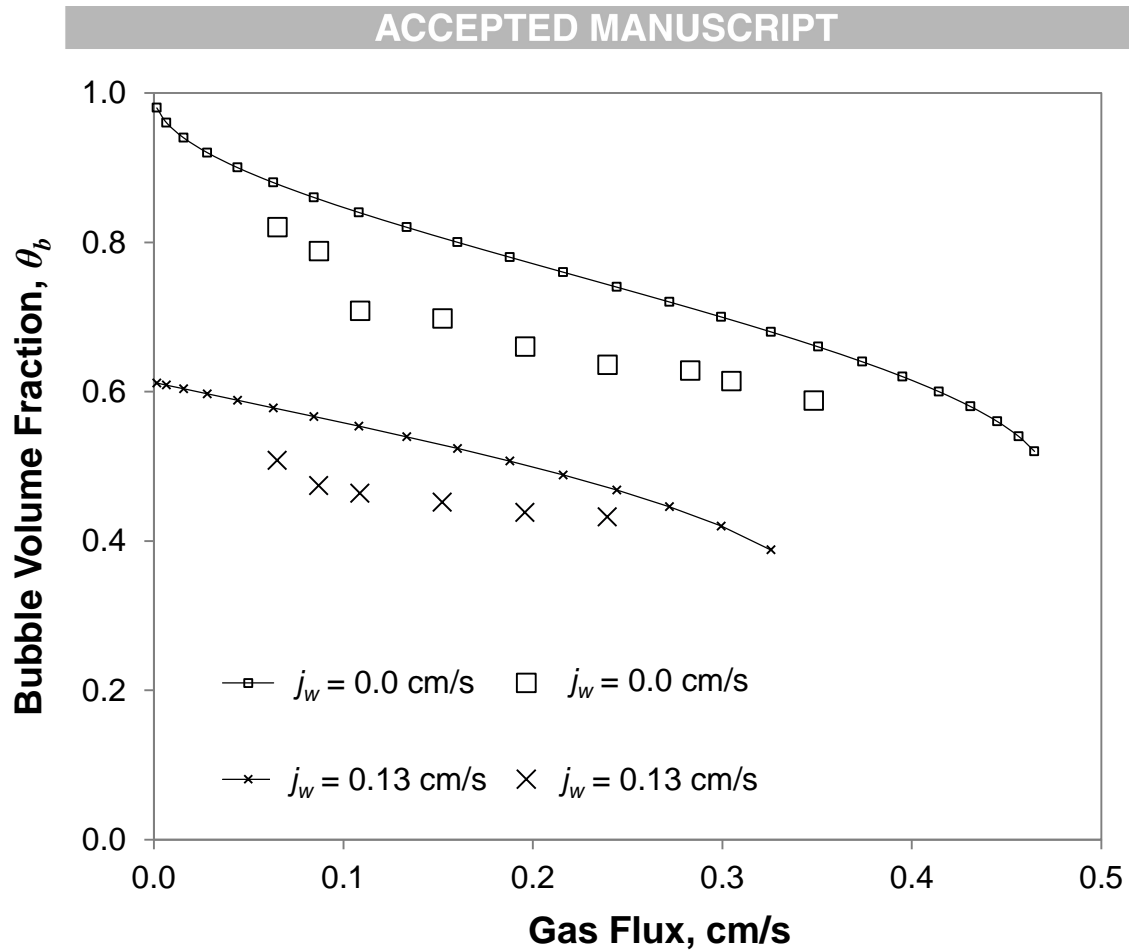


Figure 10B: The volume fraction of bubbles beneath the fluidization water inlet versus the imposed gas flux. Here the fluidized bed was positioned above the downcomer outlet. The curves for each data set are based on Drift Flux theory, with $V_t = 2.7$ cm/s and $n = 3.2$. Drift Flux theory qualitatively captures the decrease in bubble volume fraction with the addition of fluidization water.

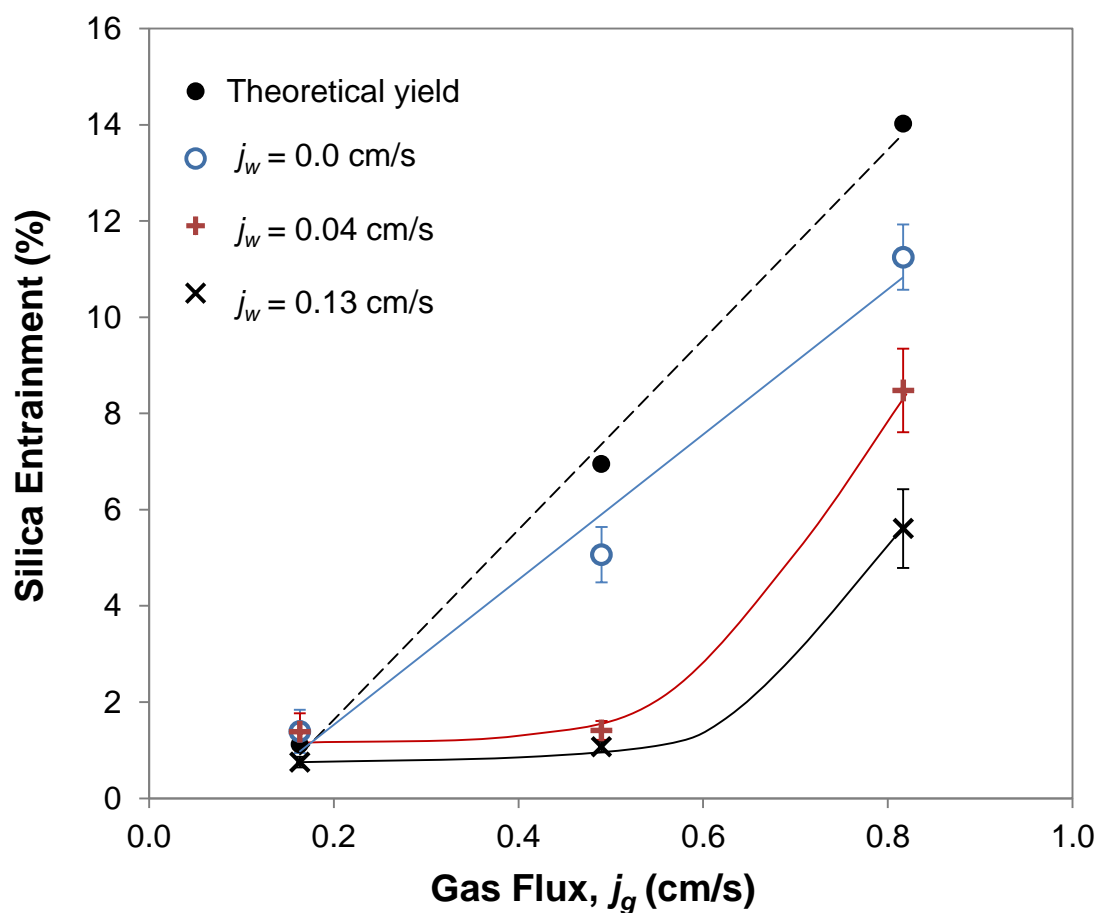


Figure 11: The entrainment of silica when operating the RFC with a fluidized bed positioned above the outlet of the downcomer. Entrainment is shown to increase with increasing gas flux, but decrease for increasing fluidization. The hypothetical hydraulic yield is based on the split of liquid in the feed to the overflow using no fluidization. Error bars are given to ± 2 standard deviations. Note the smooth curves are used to guide the eye only and are not based on the theory.

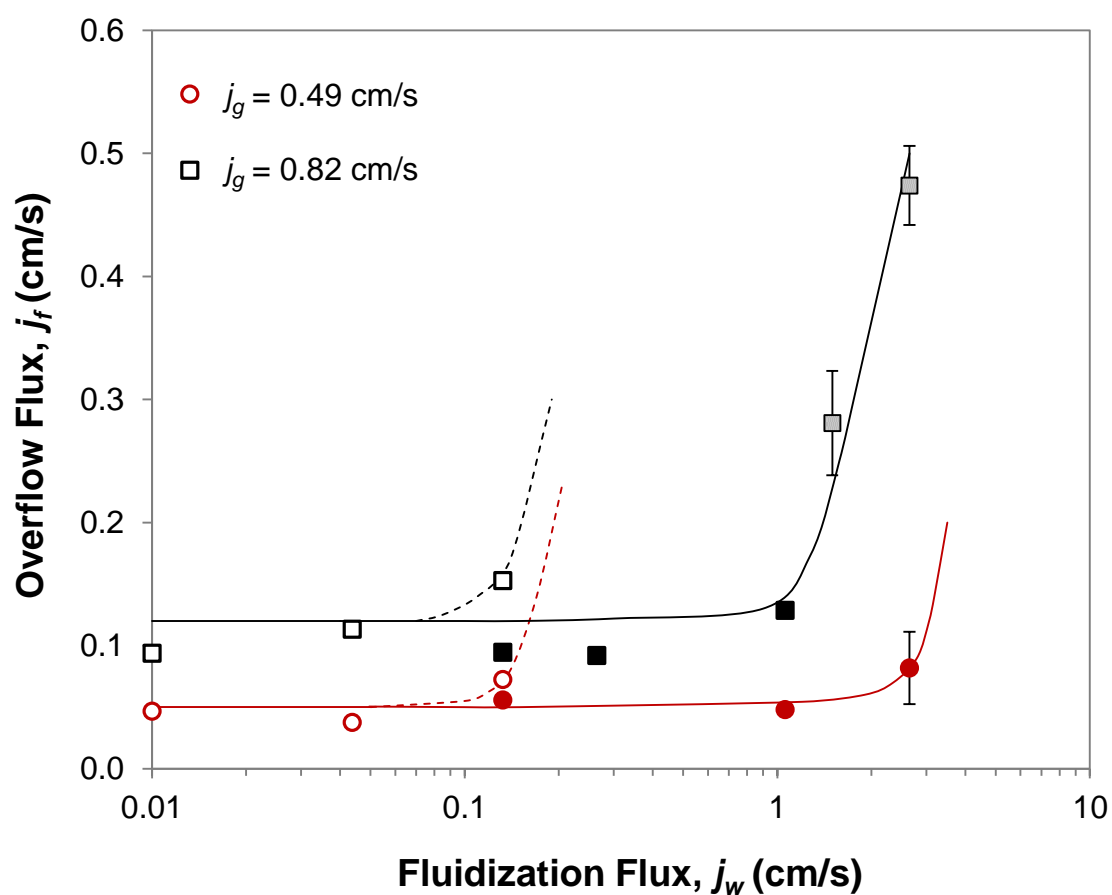


Figure 12: Liquid overflow flux versus the fluidization flux. The unfilled symbols indicate that the system was operated with the “wet” foam held above the outlet of the downcomer. The filled symbols indicate that the system was operated with the “wet” foam lowered down into the channels. Note, at the fluidization flux value of 0.01 cm/s the data corresponding to no fluidization are shown. This result has been added for completeness. Note the smooth curves are used to guide the eye only and are not based on the theory.

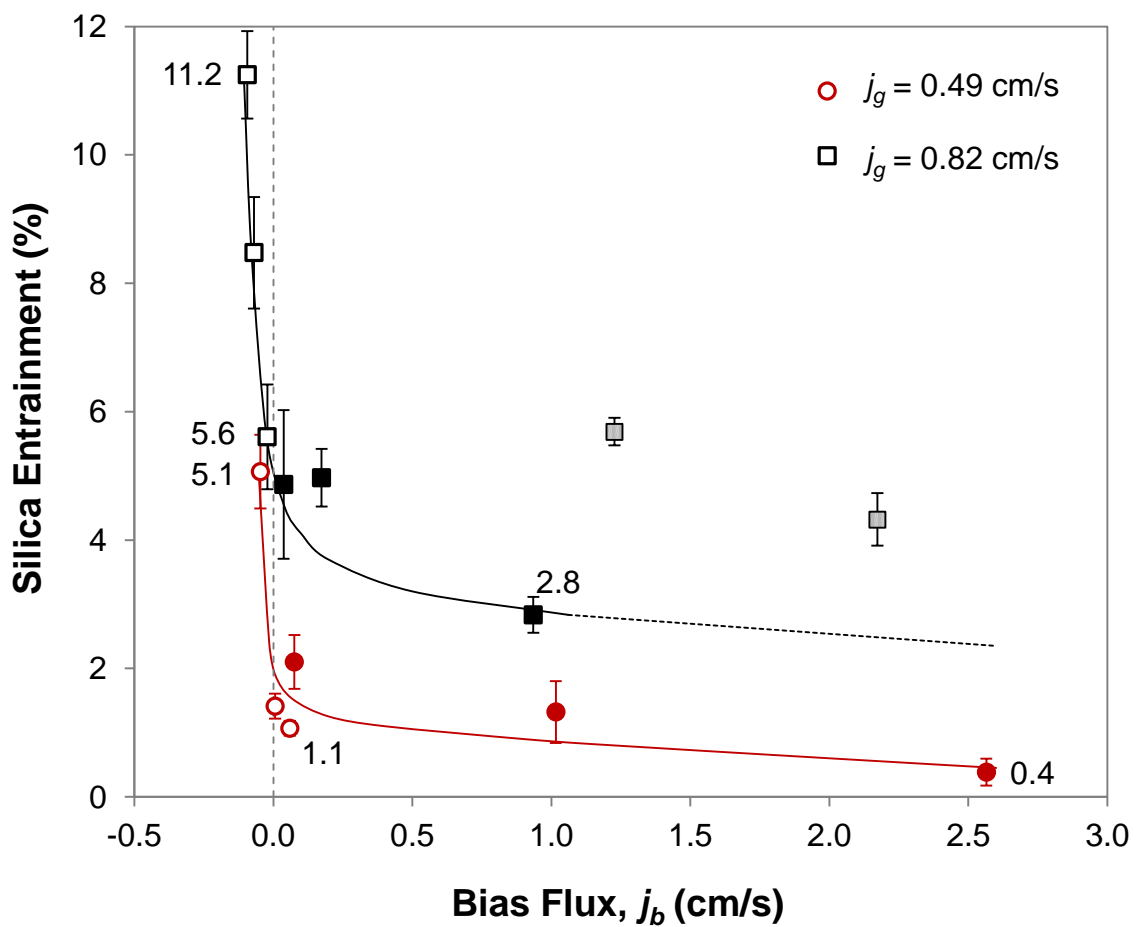


Figure 13: Silica entrainment obtained using feed slurry containing 1.6 % solids. The data are for two gas fluxes and are reported as a function of the bias flux, which is largely governed by the level of fluidization water. Unfilled symbols denote when the “wet” foam was located above the downcomer outlet. Conversely the filled symbols denote “wet” foam that entered the inclined channels. The shaded symbols denote cases when the segregation capacity of the inclined channels was exceeded. In these cases higher overflow liquid fluxes were needed in order to prevent bubble losses to tailings. Note the smooth curves are used to guide the eye only and are not based on the theory.

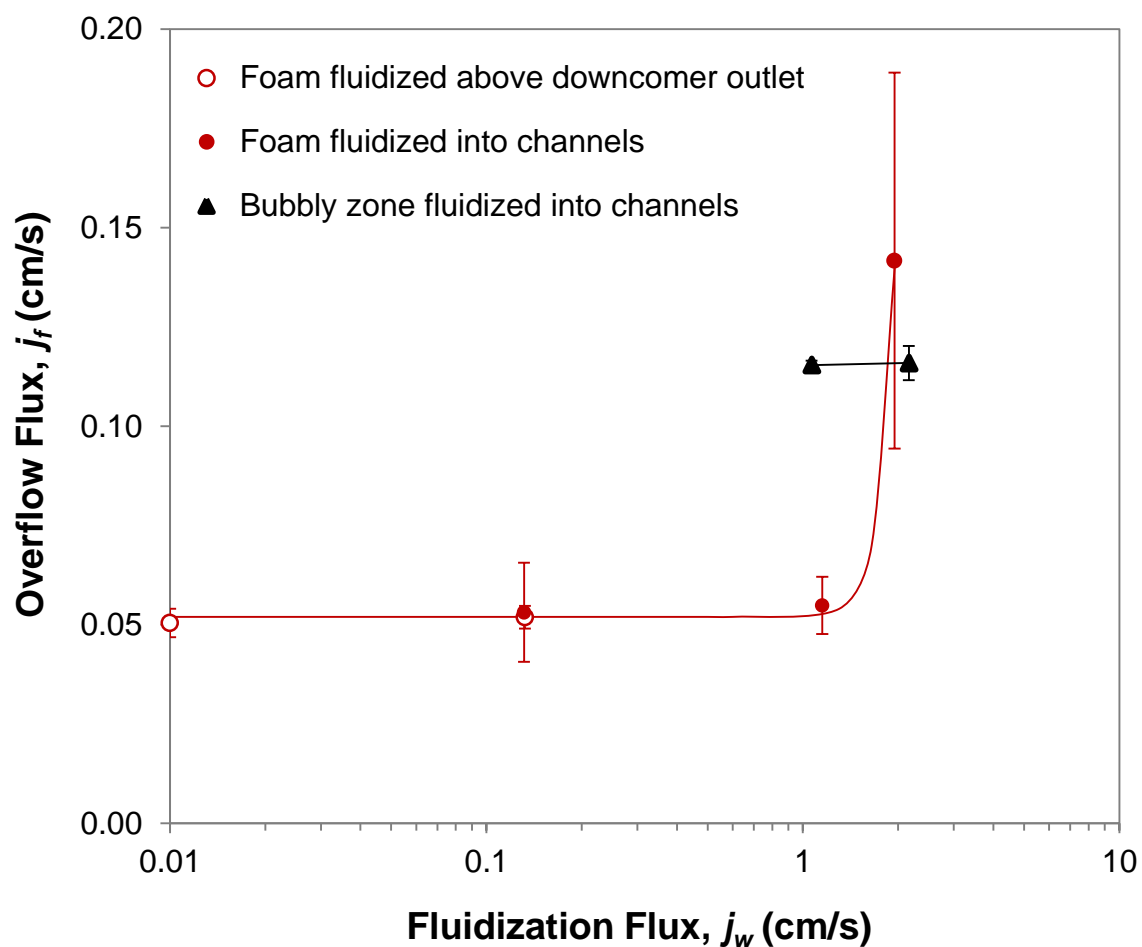


Figure 14: Overflow liquid flux obtained using a feed pulp density of silica of 6.5 % solids, and gas flux of 0.49 cm/s. The overflow liquid flux is shown as a function of the fluidization flux. There is a sudden increase that arises when the capacity of the inclined channels is exceeded. Note the smooth curves are used to guide the eye only and are not based on the theory.

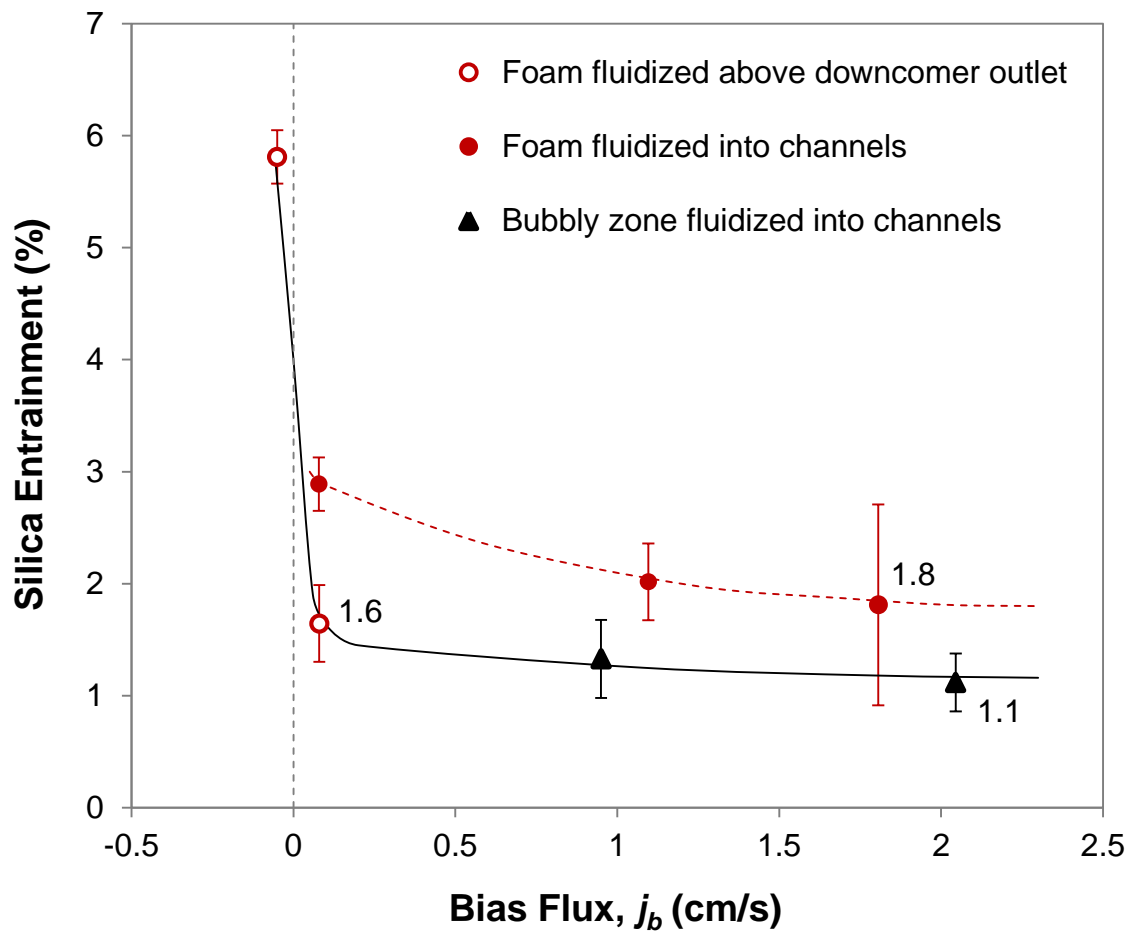


Figure 15: Silica entrainment obtained using feed slurry at 6.5 % solids and gas flux of 0.49 cm/s. The entrainment decreased rapidly as the bias flux increased, i.e. as the water fluidization flux increased. The unfilled symbols denote conditions involving a “wet” foam zone located above the inclined channels. There are two main cases. The first, denoted by the dash curve, involves foam that is introduced into the system of inclined channels, and the second, denoted by the firm curve, involves the introduction of a bubbly zone into the system of inclined channels. The bubbly zone is more permeable and thus achieves more desliming. Note the smooth curves are used to guide the eye only and are not based on the theory.

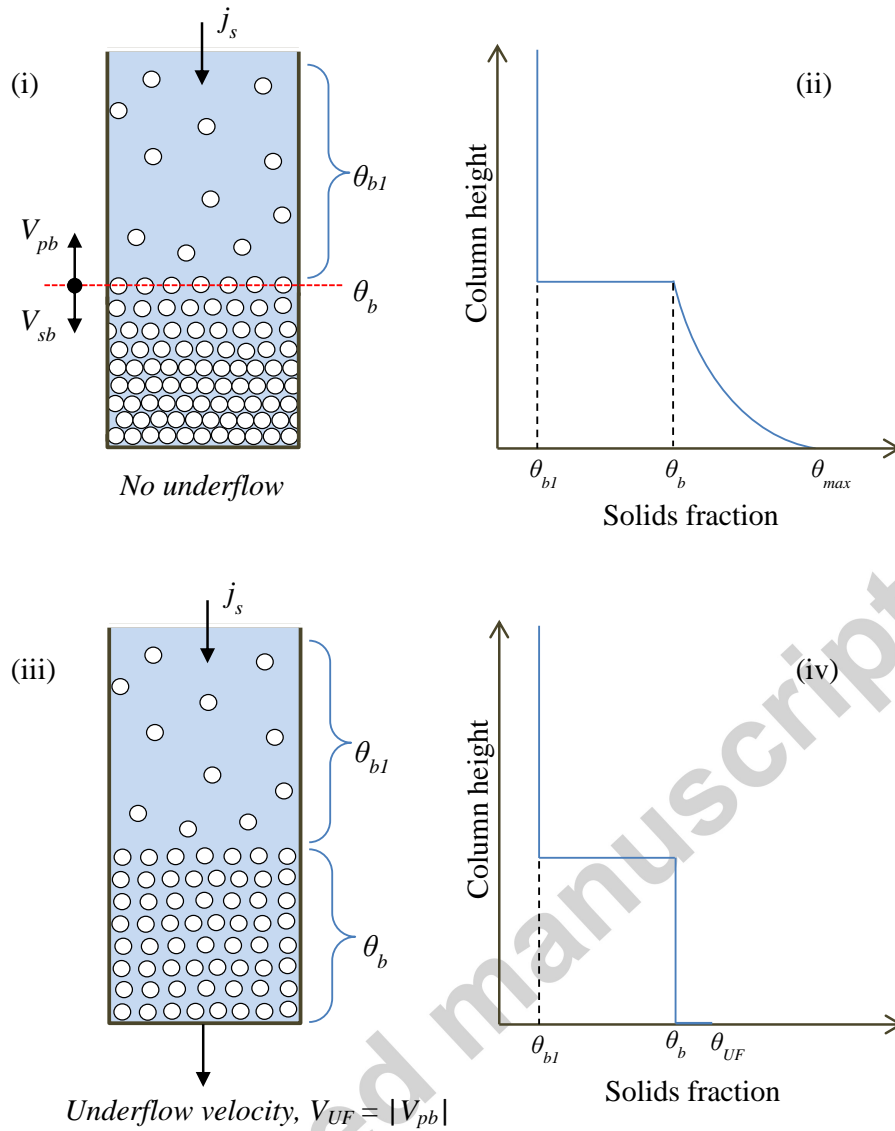


Figure A1: (i) Batch settling test with no underflow discharge. (ii) Variation in the solids volume fraction along the vertical height of the vessel at a finite time during batch settling. (iii) Particles settling with the underflow discharged at a velocity of magnitude equal to the propagation velocity defined by solids fraction θ_b . Note that the velocities are based on a fixed vessel area. (iv) At steady state a step change in solids fraction exists between the free-settling zone, the sediment bed, and the underflow concentration.

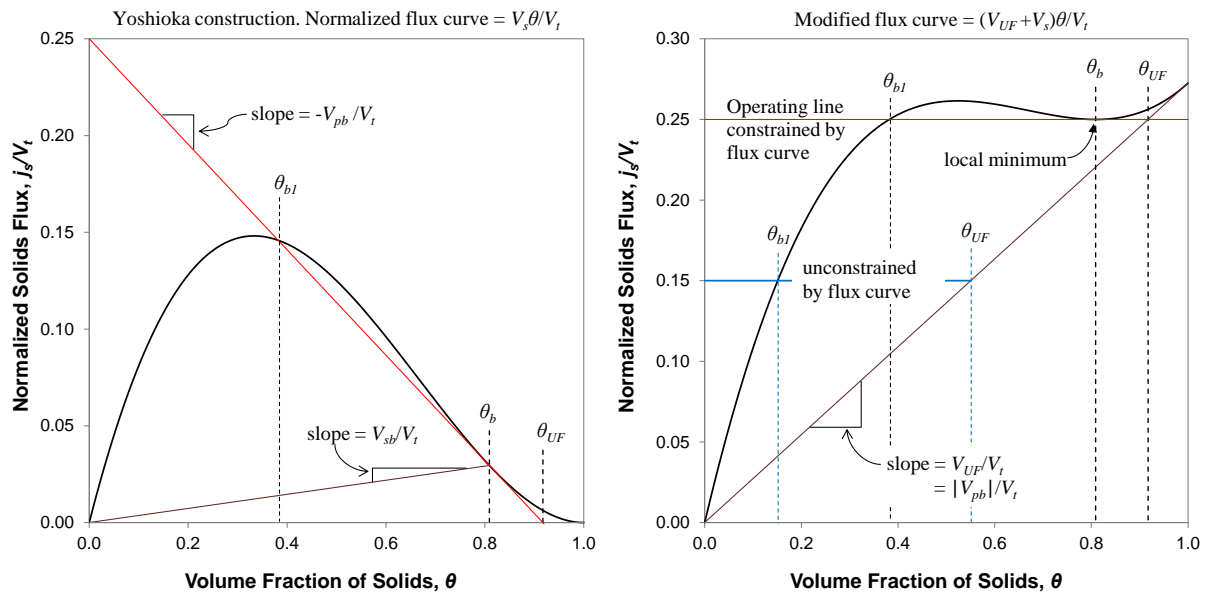


Figure A2: Flux curves used to describe batch settling and continuous steady state thickening. Note that V_s is defined by Equation 1, with $n = 2$. On the left is the Yoshioka construction, with an operating line drawn from the normalized solids flux to the curve as a tangent. On the right is the modified flux curve, with the settling rate increased by the underflow velocity. This construction provides the local minimum, which denotes the maximum solids flux that can be transported to the underflow. This construction only applies to one underflow velocity.